5

Role and Applications of Electrostatic Effects on Nucleic Acid Conformational Transitions and Binding Processes[1]

Jeff D. Ballin and Gerald M. Wilson
Department of Biochemistry and Molecular Biology,
University of Maryland School of Medicine
USA

1. Introduction

Processes involving nucleic acids are in general highly salt concentration dependent. Equilibrium binding constants (K_{obs}, defined in terms of the concentrations of the reactants and products) describing the association of proteins or multivalent ligands with nucleic acids (NAs) exhibit large negative power dependences on salt concentration. For the reaction of a ligand L with charge Z_L forming a complex with a DNA strand having Z_D phosphates,

$$L^{Z_L+} + DNA^{Z_D-} \xleftrightarrow{K_{obs}} complex \ , \tag{1}$$

the binding constant is proportional to an approximately constant power of the univalent salt concentration [MX] present in solution,

$$K_{\mathrm{obs}} \propto [\mathrm{MX}]^{SK_{\mathrm{obs}}} \ . \tag{2}$$

Experimentally, the exponent SK_{obs} typically ranges from $\approx 0.7Z_L$ to $\approx 0.9Z_L$ for single-stranded DNA (ssDNA) and double-stranded DNA (dsDNA), respectively, when $Z_D >> Z_L$ (Lohman & Mascotti, 1992; Mascotti & Lohman, 1990; Record et al., 1976). Helix formation between two complementary single-stranded NAs is also a binding process. Though the binding constant for this process is difficult to measure directly, the positive dependence of the thermal denaturation temperature on ln[salt] indicates that the strand binding constant must have a very strong positive power dependence on salt concentration (Record et al., 1998). Numerous detailed experimental and theoretical studies have characterized the binding of various positively charged ligands to polymeric NAs (Record et al., 1998). Those interactions are biologically significant in their own right and are of interest as models for protein-nucleic acid interactions which play critical roles in gene expression and replication.

[1] The preparation of this chapter was supported by NIH-NCI grant R01 CA102428 (awarded to G.M.W.) and based in part on Ballin, J.D. (2003) "Binding studies of model oligopeptides to nucleic acids: DNA length dependence, coulombic end effect, and amino acid composition effects," PhD dissertation, University of Wisconsin-Madison.

Much of the current research into protein-nucleic interactions focuses on specific complexes associated with these various processes. With the increasing ease and cost effectiveness of oligonucleotide and oligopeptide synthesis, many research laboratories use oligomers (*e.g.*, "cognate sequences," "binding motifs," and "recognition modules") to investigate binding interactions of larger *in vivo* systems (*e.g.*, plasmids, chromosomal DNA, etc.). Do these oligomers accurately model the behavior of the polymeric biological ensemble?

To answer this question, we must first ask how the binding behavior of a short oligonucleotide compares to that of longer NA lengths found *in vivo*. If differences exist between short *vs* long NAs, length dependences should be seen in the properties and processes involving short *vs* long NAs. Theory predicts and experiments show length-dependent effects influence a variety of nucleic acid properties including denaturation stability of double helices and binding of cationic oligopeptides (see Section 3). These length dependences can be ascribed to "end" effects which exert a greater effect on the observable (*i.e.*, average) properties of the nucleic acid as its chain length is reduced. In contrast, if a polymer is long enough, the terminal regions represent an insignificant fraction of the lattice and any observed interaction or process will be dominated by the interior region of the polymer (unless the phenomenon studied is specific to the ends). Therefore, if the behavior of the ends differs from that of the central region, these differences should become evident at shorter lengths.

Two kinds of end effects have been investigated for nucleic acid helices: a base stacking end effect and a coulombic end effect. A base stacking end effect in native DNA, either as a two-stranded duplex or a single-stranded hairpin, stems from a reduced stabilization of a base pair at the terminus because it has only one base stacking interaction while all interior bases have two. As a result, the stability per base pair at a given salt concentration, measured in terms of a change in standard free energy ($\Delta G°$) or the thermal denaturation temperature (T_m), decreases with decreasing chain length for a series of homologous sequences. In melting experiments, this base stacking end effect is exhibited for long NAs as a "fraying" of the terminal regions which occurs prior to denaturation of the interior double helix. These end stacking effects are contrasted with coulombic end effects caused by a difference in salt ion-NA interactions which manifest as a change in the extent of per phosphate counterion accumulation and coion exclusion[2] near the ends *vs* the NA lattice interior. While there is no dispute over the existence and consequences of a base stacking end effect on stability, the possibility of observable coulombic differences near the NA termini relative to the NA interior has been a more contentious issue. There are two sides to this debate: those who conclude that coulombic interactions with the terminal *vs* interior DNA regions (and thus between the averaged properties of "short" versus "long" polyions) have dramatic consequences on experimentally observable phenomena and those who hold that these coulombic differences have no significant impact on processes within the salt concentration range used in most experiments. Both camps can point to experimental and theoretical results that support their arguments. Is there a coulombic "end effect"? Does a charged species interact differently with the terminal regions *vs* interior of a polyion?

In order to understand the significance and differences in the behavior of polyelectrolytes attributable to coulombic end effects, one must understand how systems behave in the absence of end effects. While a survey of all relevant studies is beyond the scope of this

[2] "Counterion" and "coion" of a salt are defined relative to the (negative) nucleic acid charge. Therefore, "counterions" represent the positively charged salt cations and "coions" are the salt anions.

review, important experimental and theoretical methods that define electrostatic processes with be introduced, summarizing seminal historical studies and referencing current literature which provides technical details on the use these approaches. Where appropriate, the reader will be referred to review articles dedicated to subtopics touched upon here if more information is desired. We begin with a brief description of polyelectrolyte theories and experiments characterizing extremely long, effectively infinite, polyions. Oligoelectrolyte phenomena are discussed next, including the theories developed to explain similarities or differences observed relative to polyions. We will conclude with an overview of challenges still ahead and how they might be approached.

2. Polyelectrolyte studies

NAs are nearly ideal models of oligo- and polyelectrolytes for experimental and theoretical studies. NAs are biochemically relevant, relatively easy to manipulate experimentally, stable under a wide variety of conditions (especially DNA) and available as a monodisperse species (*i.e.*, with a defined chain length or number of monomers). This section will summarize prevailing polyelectrolyte theories to provide context for experimentally observed phenomena of nucleic acid polymers, including their fundamental properties (*e.g.*, small ion NMR relaxation rates, electrophoretic mobility) and processes involving NAs (*e.g.*, thermal denaturation, small ligand binding).

Preferential interaction coefficients. The theories described below characterize the small electrolyte ion distribution around a polyion. These ion distributions fundamentally impact NA properties and interactions but have generally eluded direct measurement of spatial distribution in solution[3]. A linkage is necessary to connect theory to experiment: preferential interaction coefficients (Γ) correlate ion concentration gradients to thermodynamic properties and therefore provide a convenient conduit from calculation to experimental observable and vice versa (Anderson & Record, 1993). Within this framework, the thermodynamic interactions of a given component or ion (*e.g.*, counterion) with some other component or species (*e.g.*, DNA) can be described simply.

Considering equilibrium dialysis as an example, the preferential interaction coefficient, Γ, characterizing salt-polyelectrolyte component interactions is defined as

$$\Gamma \equiv \lim_{C_3 \to 0} \left(\frac{\partial C_3}{\partial C_u} \right)_{T,\mu_1,\mu_3}, \tag{3}$$

where C_3 is the salt ion concentration, C_u is the molar concentration of singly charged monomer "units" (*e.g.*, NA phosphate charges), T is temperature, and μ_1 and μ_3 are the chemical potentials of the solvent and salt respectively (Anderson & Record, 1995). Preferential interaction coefficients (or if a process is considered, the stoichiometrically-weighted differences in Γ for the products and reactants) are easily related to the effects of salts and uncharged solutes on properties such as equilibrium dialysis coefficients or osmotic coefficients for processes including nucleic acid thermal denaturation studies and NA-ligand binding of biopolymers (Anderson & Record, 1983; Anderson & Record, 1993). These relationships will be discussed as their use becomes relevant.

[3] Recent developments in small-angle x-ray scattering (SAXS) and buffer equilibration-atomic emission spectroscopy (BE-AES) have yielded insights into the arrangements and distributions of ions around nucleic acids. See Section 3.2.2.

How is Γ determined? Preferential interaction coefficients for NA-containing systems can be calculated directly from grand canonical[4] Monte Carlo (GCMC) simulations performed at constant salt activity, a_3 (Mills et al., 1986). After evaluating C_3 for a series of GCMC simulations with varying C_u, Γ can be obtained from the slope of $C_3 - C_3^o$ *vs* C_u, where C_3^o is the salt concentration in the absence of the polyion (Olmsted et al., 1989; Olmsted et al., 1991) (See Section 2.2.3). Alternatively, single-ion preferential interaction coefficients expressed per polyion charge (with subscript *u* for "unit") may be obtained by integrating the ion distributions over the cell volume (V) containing the polyion (Ni et al., 1999):

$$\Gamma_{s,u} = \frac{1}{|Z_p|}\int (C_s - C_{s,bulk})dV \,, \tag{4}$$

where C_s is the local coion concentration and Z_p is the total polyion charge[5]. If a coion with valence z_s is assumed to obey a Boltzmann distribution dictated by a mean-field electrostatic potential, φ, the local coion concentration C_s can be obtained by

$$C_s = C_{3,bulk} e^{-\frac{\varphi z_s}{kT}} \,. \tag{5}$$

Using cylindrical symmetry coordinates together with eq 5, eq 4 becomes

$$\Gamma_{s,u} = 2\pi b \int C_{3,bulk}\left(e^{-\frac{\varphi z_s}{kT}} - 1\right) r dr \,, \tag{6}$$

where b is the average charge separation on the polyion. The potential φ is commonly modeled by the Poisson-Boltzmann equation, eq 11 (Misra & Draper, 1999; Ni et al., 1999; Sharp, 1995; Sharp et al., 1995; Shkel et al., 2000; Stigter & Dill, 1996) (see Section 2.2.1).
Note that the Γ in eq 3 describes the interaction of the electroneutral salt (*e.g.*, NaCl) with the polyelectrolyte (*e.g.*, NA), while eq 4 and eq 6 refer to specifically $\Gamma_{s,u}$, the coion (*e.g.*, Cl^-) preferential interaction coefficient expressed per polyion charge (indicated by the "*u*" subscript). By definition, when the polyelectrolyte and salt share a common ion, the coion $\Gamma_{s,u}$ and the salt component Γ are identical. Experimentally, $\Gamma_{s,u}$ is negative because coions are excluded from the vicinity of the NA polyanion. In an equilibrium dialysis experiment[6],

[4] Grand canonical Monte Carlo calculations are performed at constant temperature, mean ionic activity, and volume.

[5] The subscripts "*s*" and "*o*" for Γ specify the ion described: "*s*" indicates the coion, and "*o*" the counterion. These can be mnemonically related to "same" for coion and "opposite" for the counterion. Sometimes Γ_+ and Γ_- are used instead of Γ_o and Γ_s, respectively, when considering NA polyelectrolytes. If the polymer were a polycation, the coion obviously would be positive and the counterion negative. In this case, the subscript labels "+" and "-"should be transposed.

[6] An equilibrium dialysis chamber is separated into two compartments (α and β) by a semipermeable membrane through which small solutes (*e.g.*, salt ions) can pass but larger species (e.g., a nucleic acid) cannot. The system is allowed to equilibrate at constant temperature and pressure after the nucleic acid is added to compartment α, and the concentration of electroneutral salt is measured in each compartment. The Donnan coefficient, Γ^{exp}, is the quantitative measure of the difference in electroneutral salt concentrations per concentration of the larger species: $\Gamma^{exp} = \frac{m_{salt,\alpha} - m_{salt,\beta}}{m_{NA}}$. For

the coion would be excluded from the compartment containing the NA. Electroneutrality of the solution requires that nucleic acid charge must be neutralized by the accumulation of counterions and the exclusion of coions. Therefore, the $\Gamma_{o,u}$ describing the interaction of excess univalent salt with NA is easily determined since the valence-weighted sum[7] of single ion preferential interaction coefficients are related by

$$\Gamma_{o,u} - \Gamma_{s,u} = 1 \tag{7}$$

when expressed per polyion charge (denoted by the subscript "*u*"). Just as $\Gamma_{s,u} < 0$ reflects coion exclusion from the surface of the polyion, $\Gamma_{o,u}$ is a positive quantity, indicating that counterions are accumulated near the polyion. Because $\Gamma_{s,u}$ is readily accessible via the electroneutrality condition (*e.g.*, eq 7), subsequent discussion will generally describe phenomena in terms of coion interactions ($\Gamma_{s,u}$) by convention, since $\Gamma_{s,u}$ is equivalent to the Donnan coefficient[6]. Draper and coworkers provide a well-presented description of equilibrium dialysis and survey direct experimental approaches to measure Γ in RNA processes (Leipply et al., 2009).

Range of values of $\Gamma_{s,u}$. If there were no polyion-ion interactions in a monovalent salt solution, electroneutrality and random mixing (*i.e.*, entropy) dictate that $\Gamma_{s,u} = -0.5$ and $\Gamma_{o,u} = 0.5$. At the other extreme, strong counterion-polyion interactions which drive association of one univalent cation with every polyion charge (*e.g.*, NA phosphate) would exhibit $\Gamma_{s,u} = 0$ and $\Gamma_{o,u} = 1$. In practice, helical DNA at 0.0095 M sodium bromide has an experimental Donnan coefficient of -0.122 ± 0.004 (Strauss et al., 1967), reflecting the high nonideality of NAs in which a significant fraction of the counterions behave as if associated with the polyanion ($\Gamma_{o,u} \approx 0.9$). The nonideality decreases as salt concentration increases: $\Gamma^{exp} = -0.272 \pm 0.008$ at 0.23 M NaBr, and $\Gamma^{exp} = -0.538 \pm 0.0037$ at 0.98 M NaBr (Strauss et al., 1967).

2.1 Polyelectrolyte theory

2.1.1 Polyelectrolytes are surrounded by steep local ion concentration gradients

All polyelectrolyte theories for infinitely long highly charged polyelectrolytes predict the existence of steep salt ion concentration gradients (counterion accumulation and coion exclusion) in the radial direction near the surface of the polyion (*Fig.* 1). These concentration gradients are maintained by the electrostatic potential field resulting from a high axial density of structural charges (Anderson & Record, 1995). At 10.6 mM salt, native dsDNA with an axial charge density of two phosphates per 3.4 Å has a local[8] counterion concentration of about 3 M, while the coion concentration is approximately 20 μM (Ni et al., 1999). At 0.21 M salt, the local counterion concentration approaches 5 M, while the coion concentration is only 10 mM (Ni et al., 1999). These concentration gradients decay radially to the bulk salt concentration over a distance of ~ 50 Å. Gradients become less pronounced as the bulk solution salt concentration is increased. The concentration of salt ions near the

---

sufficiently dilute nucleic acids, Γ^{exp} converges to Γ (eq 3). Under all conditions considered in this chapter, the preferential interaction coefficient Γ is numerically equivalent to the Donnan coefficient Γ^{exp} (Record et al., 1998).

[7] For a polyanion in the presence of a 2:1 salt (*i.e.*, with a divalent cation and univalent anion), electroneutrality requires $2\Gamma_{2+,u} - \Gamma_{-,u} = 1$. If the polyanion solution contains a mixture of univalent and divalent cations with a shared univalent anion, charge balance requires $\Gamma_{+,u} + 2\Gamma_{2+,u} - \Gamma_{-,u} = 1$.

[8] "Local" concentration is the concentration of a given species at the surface of the polyion.

surface of the DNA increases slowly with increasing bulk salt concentration (Mills et al., 1986; Ni et al., 1999). As the bulk salt concentration increases, the local/bulk ion concentration ratio decreases and the thermodynamic nonideality contributed by salt-DNA interactions therefore diminish.

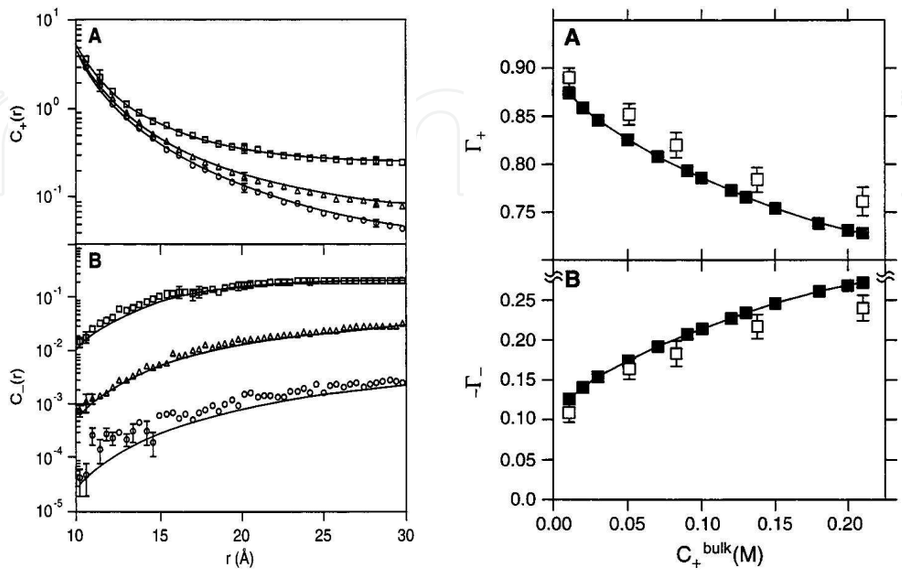

Fig. 1. (*left panel*) Dependence of monovalent cation ($C_+(r)$) and anion ($C_-(r)$) molar concentrations as a function of radial distance, r, from axis of a cylindrical model of dsDNA as derived from Monte Carlo (open symbols) and Poisson-Boltzmann calculations (smooth curves) for bulk salt concentrations of 10.6 mM (○), 51.0 mM (Δ), and 210 mM (□). (*right panel*) Canonical Monte Carlo (□) or Poisson-Boltzmann (■) calculated preferential interaction coefficients for a univalent cation (Γ_+) or univalent anion (Γ_-) with dsDNA as a function of the bulk cation concentration (C_+^{bulk}). (Figures adapted from Ni et al., 1999)

2.1.2 Important parameters in polyelectrolyte theory

When NAs are modeled as "primitive" cylindrical polyanions possessing a uniform charge distribution, polyelectrolyte behavior can be predicted using only a small number of structural parameters. The two most important parameters are the distance of closest approach between ion center and polyelectrolyte axis, *a*, and the average spacing of adjacent charges projected on the polyion axis, *b*. Often, primitive polyelectrolytes are described by the reduced axial charge density, ξ:

$$\xi = \frac{e^2}{\varepsilon bkT} . \tag{8}$$

The electron charge *e* and Boltzmann factor *k* are constants, and the product of temperature *T* and dielectric constant ε is approximately constant in water. As a result, the reduced axial charge density is almost exclusively determined by the projected axial charge spacing, *b*, with ξ = 7.14 Å/*b* in water at 25 °C. In the limit of infinite polyion dilution, counterion condensation theory (*c.f.*, Section 2.2.2) relates ξ to the preferential interaction coefficient (Manning, 1969):

$$\Gamma^{LL} = -\frac{1}{4\xi}\,\xi, \qquad \xi > 1, \tag{9}$$

where "LL" stands for "limiting law." Γ^{LL} is determined only by b: for dsDNA in water at 25 °C, Γ^{LL} = -0.06. The effective polyion radius, a, figures prominently in Poisson-Boltzmann and Monte Carlo calculations and is sometimes adjusted to account for hydration or penetration of small ions into helical grooves (see Sections 2.2.1, 2.2.2 and 3.1.2).

Correlation of the Debye parameter κ to solution behavior. The Debye parameter, κ, describes the charge screening characteristics of the solution containing the polyelectrolyte. It is dependent on the concentrations of all charged species including the polyion[9] through the ionic strength parameter, I:

$$\kappa^2 = \frac{8\pi N_A e^2 I}{1000\varepsilon kT}, \tag{10}$$

where N_A is Avogadro's number and I is ionic strength (I = 0.5Σ $z_i^2 C_i$ in which z_i is the charge of the ith ionic species and C_i is its molar concentration). At 25 °C in water, κ = (1/3) $I^{0.5}$Å^{-1}. For an infinitely dilute polyion in solution with a univalent salt possessing a common counterion, ionic strength is the same as the bulk salt concentration. Determining κ provides the necessary information to perform PB calculations on solutions of z_+:z_- symmetrical salts (eq 12). If employing the Debye-Hückel approximation (eq 15) or counterion condensation theory, κ parameterizes calculations for solutions containing salt ions of any valence.

2.2 Implementations of polyelectrolyte theory

Poisson-Boltzmann (PB) theory, counterion condensation (CC) theory, and Metropolis Monte Carlo (MC) simulations are the most common theoretical methodologies used to describe polyelectrolyte behavior. Each has advantages and limiting assumptions and all are still heavily used to describe and predict NA phenomena. After a brief overview of the concepts behind these approaches, their predictions will be compared to experimental studies of polyelectrolytes.

2.2.1 Poisson-Boltzmann equation

The PB formalism is the union of the Poisson equation with the Boltzmann distribution. For any arrangement of macroscopic or atomic charges, the Poisson equation relates the local electric potential, $\varphi(\vec{r})$, to the local charge density[10], $\rho(\vec{r})$, as a function of distance $\vec{r}$ from the polyion:

$$\nabla^2\varphi(\vec{r}) = \frac{4\pi\rho(\vec{r})}{\varepsilon}, \tag{11}$$

[9] The polyion concentration is defined as the concentration of its charged units. For example, if the polyion is a NA, the concentration is determined in terms of NA phosphate concentration.

[10] $\rho(\vec{r})$ is the net charge density of the surrounding ion atmosphere, determined by their concentrations and valences.

where ε is a spatially invariant dielectric constant[11]. The Boltzmann distribution relates local ion concentrations at a given radial distance from the polyion axis to the bulk solution ion concentration far from the polyion, based on the reduced electrostatic potential experienced at that given position. For a solution containing a polyion at infinite dilution in the presence of a symmetrical electrolyte (z_+:z_-) described by the Boltzmann distribution, the Poisson equation requires

$$\frac{\partial^2 y}{\partial r^2} + \frac{1}{r}\frac{\partial y}{\partial r} = \kappa^2 \sinh y \tag{12}$$

with the "Gauss' law" boundary conditions

$$\left.\frac{\partial y}{\partial r}\right|_{r=a} = -\frac{2z\xi}{a}, \qquad \left. r\frac{\partial y}{\partial r}\right|_{r=\infty} = 0 \tag{13}$$

when using cylindrical coordinates and the reduced potential $y \equiv ze\phi/kT$ in terms of the electron charge, e (Anderson & Record, 1990). Exact analytical solutions for the cylindrical PB equation (suitable for a stiff polyion like DNA) are known only for salt-free DNA solutions (*i.e.*, no added salt) in which all counterions have the same valence. However, by assuming that the potential of the mean force is approximated by the mean potential, the Poisson-Boltzmann equation can be applied to systems with a wide range of salt concentrations. This so called "PB approximation" has been justified on theoretical grounds for a cylindrically modeled DNA polyion at univalent salt concentrations below 0.1 M (Fixman, 1979). However, the PB approximation is likely to be more broadly applicable since numerous nonlinear Poisson-Boltzmann (NLPB) calculations using this approximation have made quantitative thermodynamic predictions that agree within ≈10% of experimental values, well inside of error, for RNA and DNA processes in up to 1 M salt (Bond et al., 1994; Korolev et al., 1998; Shkel et al., 2000; Shkel & Record, 2004).

Thermodynamic consequences can be predicted once the position-dependent electrostatic potential in hand. For example, ion gradients, measured as ratios of local (surface) to bulk concentrations, are determined by the exponential of the reduced potential. For a negatively charged polyion in solution with a 1:1 salt,

$$\frac{{}^{loc}C_+}{{}^{bulk}C_+} = \frac{{}^{bulk}C_-}{{}^{loc}C_-} = e^y \tag{14}$$

where ${}^{bulk}C_+ \cong {}^{bulk}C_-$ in excess salt. The reciprocal nature of the local versus bulk concentration ratios is a consequence of the sign inversion in y reflecting the ion charge z for cations *vs* anions. Eq 14 indicates that counterions are accumulated and coions are excluded from the polyelectrolyte surface (Ni et al., 1999). An increase in bulk salt concentration results in a much larger fractional increase in ${}^{bulk}C_+$ and ${}^{bulk}C_-$ than the increase in ${}^{loc}C_+$ and ${}^{loc}C_-$. Other thermodynamic parameters which are accessible via the reduced potential

[11] Distance-dependent dielectrics, $\varepsilon(\vec{r})$, have been used to model solvent effects (*e.g.*, dielectric saturation). Additional details and approaches are reviewed by (Grochowski & Trylska, 2008; Wong & Pollack, 2010; Wu & Morikis, 2006).

include preferential interaction coefficients (Γ) (Bond et al., 1994; Shkel et al., 2006; Shkel & Record, 2004), osmotic (ϕ) and activity coefficients (γ) (Anderson & Record, 1983; Record et al., 1978), the salt dependence of DNA denaturation (Bond et al., 1994; Korolev et al., 2002; Shkel & Record, 2004), and the thermodynamics of ligand binding phenomena (Rouzina & Bloomfield, 1997; Sharp et al., 1995; Stigter & Dill, 1996; Zhang et al., 1996). As mentioned above, experimental results have been very faithfully predicted in NLPB studies using both primitive and 3-D models of NAs. Numerous reviews detail the history, application, and comparisons of PB theory to experiment (Anderson & Record, 1995; Draper, 2008; Fogolari et al., 2002; Jayaram & Beveridge, 1996; Koehl, 2006; Wu & Morikis, 2006).

Development of the PB equation. Initial efforts to describe polyelectrolytes using PB theory relied on linearization of the potential distribution around a symmetric cylinder, an approximation valid only for very low charge density polyelectrolytes or at high salt concentration (see Section 2.2.2). The linearized PB solution is accurate when the reduced potential is small ($|y| < 1$), but does not describe dsDNA at experimental salt concentrations (*e.g.*, $y \approx 3$ at 0.1 M salt). In the decades since development of the Debye-Hückel limiting law, many asymptotic series expansion solutions have been developed to account for the high surface potential of NAs[12]. More recently, asymptotic solutions of the cylindrical PB equation for both high salt ($\kappa a \geq 1$, or more than 0.1 M univalent salt for B-DNA) (Shkel et al., 2000) and low salt ($\kappa a < 1$, or less than 0.1 M 1:1 salt for B-DNA) (Shkel et al., 2002; Trizac & Téllez, 2007) have been derived, providing explicit analytical expressions for the electrostatic potential and for the resulting preferential interaction coefficients, covering the entire experimental salt concentration range accessible to the PB formalism. These analytical expressions have calculated Γ for single, double, and even triple-stranded NAs with error small enough for comparison with experiments[13]. For example, the Shkel (2000) asymptotic predictions of Γ were within 5% of numerical NLPB calculations for dsDNA at 0.1 M univalent salt, with error decreasing as salt concentration increased. Most recently, a single analytical expression has been developed which predicts the electrostatic free energy of a polyelectrolyte within 2% of NLPB calculations for either a primitive cylinder or for 3-D models of B-DNA obtained from the Protein Data Bank (Shkel, 2010).

Difference between "primitive" cylindrical and structurally detailed 3-D models in NLPB calculations. Early polyelectrolyte studies by necessity considered only "primitive" representations of NAs (*e.g.*, lines of charge, cylinders, planes, etc.). With the advent of more detailed biomolecular structural information, more powerful computational resources and the availability of commercial and open-source PB calculation packages (such as DelPhi, APBS, and MEAD; see (Koehl, 2006) for additional details), Poisson-Boltzmann analyses using detailed 3-D models have become widespread in the literature. Not surprisingly, NLPB calculations employing NA models with atomic resolution have come into vogue as well (Chen & Honig, 1997; Grochowski & Trylska, 2008; Koehl, 2006; Misra et al., 1994; Sharp et al., 1995). With these developments, the minimum detail necessary to accurately describe experimentally relevant systems has come under debate. Proponents of highly detailed models have implied that such detail is necessary to predict phenomena accurately (Chen & Honig, 1997; Jayaram & Beveridge, 1996). Advocates of the "stripped down" (*e.g.*,

[12] Shkel *et al.* (2000) reviews several asymptotic approaches to the Poisson-Boltzmann equation.

[13] "Error" is defined in this case as the difference $\Gamma_{analyticalPB}$ - Γ_{NLPB} calculated for a cylindrical or spherical model.

cylindrical) approach (Anderson & Record, 1995) claim that simplified polyelectrolyte models capture the essence of thermodynamic phenomena under typical experimental conditions and often predict results with quantitative agreement to experiment. They point out that the lack of structural details available for some systems[14] may result in inconsistent modeling due to differences in the level of detail incorporated for the components in a given study.

To assess how inclusion of additional structural complexity might impact experimentally accessible predictions, calculations of Γ were compared for cylindrical and all-atom polyions in the presence of 0.1 M univalent salt (Sharp, 1995). Relative to a primitive cylinder model, a detailed 3-D model of DNA exhibited ~5% less counterion accumulation around the DNA due to the helical charge arrangement and groove structure. The reduced counterion accumulation resulted in a small but significant difference in the Donnan coefficient (Γ_{3D} - $\Gamma_{cyl} \cong$ -0.028 at 1 mM salt) which decreased $\lesssim$ 2-fold as salt increased in the 1 – 100 mM salt concentration range considered[15]. The salt dependence of Γ was otherwise comparable using either the cylindrical or structurally detailed DNA models. In a subsequent paper, NLPB calculations modeling the binding of DAPI with DNA as a cylinder-sphere interaction were compared with those employing an all-atom model for the complex (Sharp et al., 1995). The predicted salt dependence of binding, SK_{obs} (eq 20), from the two models were within 3% of each other (-1.9 *vs* -1.95 respectively[16]). More recently, comparison of free energy calculations of the cylindrical free energy with that calculated for the all-atom structural model of linear B-DNA found that that the cylindrical model is completely sufficient for 1:1 (monovalent) salt concentrations above 0.01 M (Shkel, 2010).

On the other hand, study of extreme phenomena such as highly complex nonperiodic geometries, large dynamic macromolecular structural changes, or very high salt concentrations, may require structural detail. For example, NLPB thermodynamic predictions of DNA operator binding by the λ repressor N-terminal domain (λbd) yielded significantly different results when comparing a cylinder-sphere model *vs* using the λbd-DNA complex crystal structure coordinates: SK_{obs} = -1.9 *vs* -4.7, respectively, while the experimentally measured SK_{obs} = -4.2. However, λbd is an ampholytic protein with 24 basic residues and 22 acidic residues, with most of the cationic amino acids near the DNA binding interface and the anionic residues on the other face (Sharp et al., 1995). A 10 Å sphere with a net +2 charge is a poor model for a protein with 46 charges and ignores, as the authors noted, the "polyelectrolyte" character of the protein. In another study, the non-uniform topology of DNA (*e.g.*, the presence of grooves) becomes important at very high salt or close proximity to the DNA surface (Montoro & Abascal, 1998). In perspective, the level of fine detail required in a model is dictated by the range of the phenomena that are to be studied. Whereas atomic detail in the model may be important in a computational study investigating the role of specifically bound Mg^{2+} in ribozyme catalysis or stability, for

[14] Biological systems lacking 3-D coordinates include ssDNA and the highly flexible regions of many biomolecules.

[15] This difference was determined via interpolation from Sharp's (1995a) Figure 3b. Finite-difference 3-D PB calculations on dsDNA predict $\Gamma_{3D} \cong$ -0.11 *versus* the primitive cylinder-based Γ_{cyl} = -0.083 at 1 mM *versus* $\Gamma_{3D} \cong$ -0.19 and Γ_{cyl} = -0.21 at 100 mM salt. By comparison, idealized (infinite dilution) Γ^{LL} = -0.069 (eq 9).

[16] The experimental values were SK_{obs} =-2 for DAPI-poly[d(AT)]$_2$ and -2.3 for DAPI-poly[d(GC)]$_2$ (Wilson et al., 1990).

denaturation studies and nonspecific binding events, the primitive models predict experimental results well within error. Primitive models offer great advantages when applied to appropriate biomolecules and processes: (i) results provide accurate characterization of phenomena, often using only a few, readily understood parameters; (ii) solutions are formulated analytically and are thus easy to use; (iii) and the predicted consequences offer a generalized framework which can be applied to other systems.

Limitations of Poisson-Boltzmann approaches. Standard implementations of PB neglect ion-ion correlations between salt ions, interactions between the ions and solvent, and consider ion size (*i.e.*, volume) only as a distance-limit of closest approach to the polyion surface. The solvent is usually described with a uniform dielectric continuum or with a parameterized expression for a varying, distant-dependent dielectric[17], in either case idealizing its molecular character. At lower salt ($\lesssim$ 0.01 M 1:1 salt), the calculated potentials near the polyion surface increase strongly, numerical error becomes significant, and the calculations become more time consuming. Numerous approaches addressing these issues with varying degrees of success have been developed and are the subject of several reviews (Anderson & Record, 1990; Anderson & Record, 1995; Grochowski & Trylska, 2008; Jayaram & Beveridge, 1996; Koehl, 2006; Record et al., 1998; Tan & Chen, 2009; Wu & Morikis, 2006). Finally, standard PB approaches rely on a static model of the polyion and thus do not consider polyelectrolyte dynamics (*e.g.*, if the polyion is a writhing single-stranded nucleic acid). The increasingly active efforts to describe polyion dynamics and their interactions with surrounding ion distributions are reviewed elsewhere (Prabhu, 2005; Slater et al., 2009; Viovy, 2000).

2.2.2 Counterion condensation theory

Counterion condensation theory (Manning, 1969; Manning, 1978) was originally derived within the context of a double limit: (i) the polymer is infinite in length and therefore end effects are ignored; and (ii) the concentrations of all ionic species are made infinitely small by dilution with water but that salt is in excess over the polyion charges. CC theory simplifies the continuous ion concentration gradients near the polyion by proposing the existence of a coion-free surface region where counterions are "condensed" or "territorially bound" in close proximity to the polyion backbone but still allowed to translate along it. Counterions with a valence z_c are predicted to condense if the reduced axial charge density ξ (eq 8) of the polyion exceeds the critical value $1/z_c$ (Manning, 1969). After condensation, the actual charge density of the polyelectrolyte is reduced to an effective charge density of $\xi_{eff} = 1$. Therefore, double stranded B-DNA, with $\xi = 4.2$, is predicted to exhibit significant counterion condensation.

Counterions which are not condensed are in the "diffuse ion atmosphere" where they experience a lower electrostatic potential governed by the Debye-Hückel approximation: for a given ion configuration, the electrostatic field of ion ensemble is simply the sum of the isolated electrostatic potentials associated with each ion. However, the ion atmosphere around each charged species, *i*, causes the potential to decay more sharply with distance, creating a "screened coulomb potential" analogous to that in linearized spherical PB theory (a.k.a., Debye-Hückel theory):

[17] Typically, a distance-dependent dielectric is invoked to take into account dielectric saturation of the solvent in close proximity to charges.

$$\varphi_i = \frac{e^{-\kappa r}}{r} . \quad (15)$$

In later CC approaches (Manning, 1977; Manning, 1978), this screened potential is assumed to describe the interactions of small ions with the polyion and its condensed counterions. At distances greater than the Debye length outside the volume enclosing the polyelectrolyte and its condensed ions, the polyion looks like a line of charges whose effective charge is reduced by ξ. At distances less than the Debye length, electrostatic interactions are not fully screened. In other words, ξ determines the onset and extent of counterion condensation, while the Debye length κ^{-1} (eq 10) defines the distance over which the ion distribution affects solution properties surrounding the polyelectrolyte.

Extended CC theory. From this theoretical framework, limiting law values for colligative properties such as preferential interaction coefficients (Γ), osmotic coefficients (ϕ), and activity coefficients (γ) are easily expressed in terms of ξ (Manning, 1969). Researchers found that limiting-law predictions of experimental values still appeared numerically accurate even at salt concentrations beyond the constraints in which CC theory was derived. In particular, the effective polyelectrolyte charge fraction, $1/(z_c\xi)$, was found to be relatively constant versus salt concentration in many experimental studies (see references in (Manning, 1977; Manning, 1978)). To explain this observation, Manning (1977, 1978) extended CC theory by assuming an analytical free energy expression, *w*, defined by the "charging" energy of the DNA phosphates and the ideal mixing free energy of the various species. The fraction of ions, θ, condensed around the polyion and the volume, *V*, which contains them are obtained by minimization of the free energy expression, *w*, with respect to θ. The volume depends on the polyion characteristics ξ and *b*, the valences of the salt ions, and only weakly on the salt concentration itself. The cylindrical condensation volume for B-DNA is predicted to be *V* = 720 ml/mol-phosphate, with an outer condensation radius of approximately 17 Å for a polyion radius of 10 Å (Manning, 1977). The fraction of condensed ions, $\theta = 1 - 1/(z_c\xi)$, contained within this volume is effectively considered to be a part of the polyion and is no longer electrophoretically or osmotically active. Therefore, the condensation of θ = 0.76 univalent counterions per dsDNA phosphate reduces the magnitude of the "effective" B-DNA charge to 0.24 per phosphate. The concentration of counterions in this condensed layer exceeds 1 M (on a per mol phosphate scale, 0.76 mol counterions in a 0.72 liter volume). CC theory was recently the subject of an extensive review (Spasic & Mohanty, 2008).

Counterion condensation theory has been used to describe a wide range of salt concentration-dependent nucleic acid phenomena because its simplified picture of polyelectrolyte systems has successfully predicted at least the qualitative details of polyion thermodynamic behavior (Manning, 1978). CC theory has been applied to Donnan equilibrium (Manning, 1969), osmotic coefficients (Manning, 1969), electrophoretic mobility (Sections 2.3.2 and 3.2.3), DNA denaturation (Sections 2.3.3, 3.2.4 and 3.2.5), and ligand binding (Sections 2.3.4 and 3.2.6). Manning and coworkers (Manning, 1977; Manning, 1978) have claimed that CC theory can be successfully applied with bulk monovalent salt concentrations approaching 1 M. However, several labs dispute the accuracy of this claim (Allison, 1994; Fenley et al., 2010; Record et al., 1998; Sharp et al., 1995; Stigter, 1995). With the increased availability of powerful computational resources, more sophisticated numerical methods such as NLPB (discussed above), and molecular simulation techniques such as Monte Carlo and molecular dynamics have become increasingly more prevalent.

2.2.3 Monte Carlo simulations

Monte Carlo (MC) methods determine an equilibrium distribution of component species by making a series of stochastic rearrangements to find the energetic minimum of the system. Both the "depth" and the "broadness" of the free energy minimum are important in determining the equilibrium condition. Monte Carlo simulations have significant flexibility in system modeling and require a minimum of assumptions:

i. simulations can be as large (*e.g.*, number of species in simulation) or complicated (*e.g.*, 3-D models, discrete solvent, etc.) as desired, limited only by the amount of time and computer resources available to the researcher;
ii. MC accounts for the ion-ion correlations ignored by Poisson-Boltzmann theory;
iii. electrostatic forces are calculated directly based on the coulombic potential of discrete charges, unlike counterion condensation theory which relies on significantly simplifying assumptions (Debye-Hückel approximation to describe mobile ions; counterion condensation hypothesis).

However, the error associated with calculated ion distributions scales with the number of species (*e.g.*, ions, water molecules, etc.) due to increased stochastic noise. Early MC simulations were typically limited to less than 0.1 M salt (Olmsted et al., 1989; Olmsted et al., 1991; Olmsted et al., 1995), although more recent simulations have modeled higher salt concentrations (*e.g.*, 0.2 M (Ni et al., 1999), and 4.5 M (Montoro & Abascal, 1998)). In general, the ratio of ions/polyion or waters/polyion is limited by the cell size of the calculation.

Monte Carlo simulations make a series of random changes to a given distribution of species. The decision to keep or reject the new configuration is based on the change in system energy

$$P = e^{-\frac{E_{new} - E_{old}}{kT}}, \tag{16}$$

where E_{new} and E_{old} are the system energies of the new and old configurations respectively. If P is greater than 1, the new arrangement is kept and a new set of random moves is made. If the energy ratio P is less than 1, it is compared to a random number between 0 and 1. If P is greater than this number, the configuration is kept, otherwise it is rejected. In either case, another random move is performed. This randomized acceptance of higher energy arrangements allows the system to move out of local energy minima. Eventually, assuming "enough" iterations are executed, the ensemble average of the energy *vs* the number of steps stabilizes, reflecting a convergence to equilibrium.

Grand canonical Monte Carlo (GCMC) simulations require that the temperature, electrolyte activity, and volume of the system be specified before the simulation begins. After the number of small ions in the cell comes to equilibrium, the electrolyte concentration can be easily determined as a statistical average over fluctuations. Preferential interaction coefficients (Γ) can be extracted from these energy minimized ion distributions (Jayaram & Beveridge, 1991; Olmsted et al., 1989; Olmsted et al., 1991; Olmsted et al., 1995).

The earliest applications of GCMC simulations were used to determine activity coefficients for simple electrolytes. Since then, MC calculations have been used to determine mobile ion distributions (Montoro & Abascal, 1998; Ni et al., 1999), ion-size effects on ion-DNA interactions (Wang et al., 2007), thermodynamic coefficients (Jayaram & Beveridge, 1991; Korolev et al., 1998; Mills et al., 1986; Olmsted et al., 1991; Paulsen et al., 1987) and ligand

binding (Ni et al., 1999; Olmsted et al., 1995). Because MC simulations are considered one of the more "realistic" computational methodologies available, they have been used for comparisons with experimental results and as a reference for alternative theoretical frameworks (*e.g.*, PB or CC).

2.2.4 Comparisons between PB, CC, and MC theories with experiment

All three theories can be applied to the same structural model of polyion and solution, using either a cylinder or full 3-D model for DNA, with either a uniform dielectric or variable local dielectric continuum for the solvent (*cf.*, Table 1). Many labs have made comparisons between the three theoretical frameworks and experimental data.

In general, CC theory agrees with PB calculations at very low salt concentrations (submillimolar) or where phenomena of interest are occurring far from the polyion. PB and CC determinations of the Donnan coefficient agree with one another for infinitely dilute polyions in the presence of excess salt ($\kappa a \lesssim 10^{-3}$, or ≈100 nM univalent salt) (Anderson & Record, 1980). Analytical expressions of polyion colligative properties (*e.g.*, preferential interaction coefficients, osmotic coefficients, and activity coefficients) derived from PB theory were found to be in agreement with counterion condensation theory at low but finite salt concentrations (Klein et al., 1981). Aspects of CC phenomena predicted by Manning are seen in PB calculations for the "no added salt" limit and appear to hold true even in the presence of added salt (Le Bret & Zimm, 1984). CC and PB theory agree at radial distances greater than a Debye length from the polyion (*e.g.*, cation concentrations are indistinguishable at 60 Å at 0.01 M 1:1 salt with a = 5 Å) (Stigter, 1995). CC theory is typically effective in predicting behavior of properties which depend on long range ion-polyion interactions, such as the salt distribution observed in a Donnan equilibrium experiment. CC theory also works reasonably well for polyion processes such as nonspecific ligand binding and especially its salt dependence, both of which rely more on the overall electroneutrality of the ion distribution than the specifics of its spatial organization. Myriad examples of CC analysis applied to binding interactions are described in reviews (Anderson & Record, 1982; Manning, 1978; Spasic & Mohanty, 2008).

On the other hand, CC predictions disagree with those of PB and MC at higher salt concentrations in numerous studies which compared CC to other computational and/or experimental results (Anderson & Record, 1983; Anderson & Record, 1995; Fenley et al., 2010; Korolev et al., 1998; Stigter, 1995). For example, the number of counterions (β) within an annular shell a distance Δ from the DNA cylinder surface were compared from PB and CC calculations for $[Na^+]/[P]$ concentration ratios comparable to those typically used in NMR studies ($1.2 \leq [Na^+]/[P] \leq 9.0$) (Mills et al., 1986). Mills *et al.* found that CC theory reasonably approximates the magnitude of β within the condensation layer but fails to reproduce the increase of β with increasing salt. On the other hand, even though the lack of ion-ion correlation effects in PB calculations caused a systematically lower β prediction relative to MC, the difference ($\beta^{MC}(\Delta) - \beta^{PB}(\Delta)$) was relatively independent of salt concentration. As such, PB mirrored MC-predicted distance-dependent changes in ion distributions. Murthy and coworkers (Murthy et al., 1985) noted that PB underestimates the local Na^+ concentration around an infinite polyion by about 15% relative to MC and hypernetted chain (HNC) calculations done between 1 – 10 mM NaCl. However, PB, HNC, and MC predictions become indistinguishable at long distances from the DNA (~120 Å at 10 mM and ~360 Å at 1 mM NaCl) (Murthy et al., 1985).

Consideration	**CC theory**	**PB calculation**	**MC simulation**
Ions	considered either condensed or free; no explicit consideration of identity	no ion-ion interactions; ion radius only considered as part of polyelectrolyte cylinder radius, *a*	ions have volume; ion-ion correlations; discrete ion electrostatics
Solvent	constant dielectric continuum	constant dielectric; distance-dependent dielectric field	constant or varying dielectric; explicit water molecules
Polyion model	cylinder; line of charges	cylinder; 3-D model	cylinder; 3-D model
Electrostatic forces	linearized Debye-Hückel; minimization of free energy	continuum electrostatics (explicit charges for polyion and ligands, charge density for mobile ions) (Shkel, Trizac)	coulombic (discrete charges)
Salt concentration range	exact at 0 M univalent salt; < 1 mM salt verified; some argument for < 1 M	≤ 0.1 M theoretical limit (Fixman); ≤1 M univalent salt experimentally validated (Bond, Korolev)	< 0.1 – 0.2 M common; higher concentrations available (e.g., 4.5 M univalent (Montoro))
Approach to thermodynamic output	predict from simple picture of ion-polyion interactions; system energy is known	find potential field φ; calculate ion distribution; get thermodynamics via Γ	yields ion distribution directly; derive thermodynamics from Γ
Ease of use	very easy	moderate	moderate
Advantages	explicit analytical expression via basic parameters (ξ, κ)	well-defined distribution law; well-characterized model	Uses minimal assumptions; allows arbitrary complexity; provides estimation of error
Caveats	coarse-grained description, potentially large discrepancy for near-field phenomena	large errors when electric fields are high (*e.g.*, at high [salt]); ignores ion correlations (an issue for multivalent ions)	computationally demanding; stochastic noise increases with increasing [salt] and number of solvent molecules
Linkage to experiment	colligative properties (Γ, γ, ϕ); NA thermal denaturation; ligand binding; electrophoretic mobility	colligative properties (Γ, γ, ϕ); NA thermal denaturation; ligand binding	colligative properties (Γ, γ, ϕ); NA thermal denaturation; ligand binding

Table 1. Feature comparison of polyelectrolyte theoretical descriptions

PB and MC estimations of measurable parameters commonly agree with experiment, especially when solution conditions are amenable to PB assumptions. Paulsen *et al.* (1987) found that Γ values predicted by PB and MC calculations agree with experimental Donnan coefficients measured between 1 – 31 mM DNA phosphate and 0.2 – 111 mM NaCl.

Similarly, PB and MC approaches yielded equivalent results for Γ and mean ionic activity coefficients for a primitive DNA model in the presence of 2 – 36 mM 1:1 salt (Mills et al., 1986). Using primitive cylinders to describe polyions and lattice statistics to model flexible ligands (such as oligopeptides), NLPB calculations made accurate predictions of measured equilibrium binding constants and their salt dependences for a range of binding processes including: (i) Mg^{2+} to polynucleotides, (ii) $Co(NH_3)_6^{3+}$ to calf-thymus dsDNA, (iii) polyamines to T7 DNA, (iv) oligolysines to polyU and polyA, and (v) tripeptides to heparin, a highly charged polysaccharide (Stigter & Dill, 1996). MC and PB predictions were in excellent agreement for the change in electrostatic free energy for duplex DNA helix-coil transitions across a range of NaCl and $MgCl_2$ concentrations (Korolev et al., 1998).
However, omission of ion-ion correlations significantly decreases the predicted accumulation of multivalent cations near the polyion surface. Comparisons of PB vs MC found ~20 – 30% discrepancies in predicted local ion concentrations and Γ for systems containing divalent cations (Ni et al., 1999; Pack et al., 1999). Differences between PB and MC determinations of Γ_{2+} for polyelectrolyte solutions containing single or mixed 1:1 and 2:1 salts were attributable to a dramatically increased local cation accumulation within 3 Å of the dsDNA cylinder surface (*Fig.* 2). The net difference $\Gamma_{2+}^{MC} - \Gamma_{2+}^{PB}$ is relatively invariant across the ~10 – 200 mM univalent salt concentration range studied (Ni et al., 1999), consistent with the roughly invariant $\beta^{MC}(\Delta) - \beta^{PB}(\Delta)$ discussed previously (Mills et al., 1986). Fortunately, the relatively constant differences between predicted ion distributions cancel out for thermodynamic processes that are described by stoichiometric-weighted changes in Γ. This may explain the remarkably accurate NLPB thermodynamic predictions of diverse processes such as RNA folding (Draper, 2008), nucleic acid thermal denaturation (Shkel & Record, 2004), and ligand binding to NAs (Anderson & Record, 1995; Misra & Draper, 1999; Record et al., 1998; Stigter & Dill, 1996).

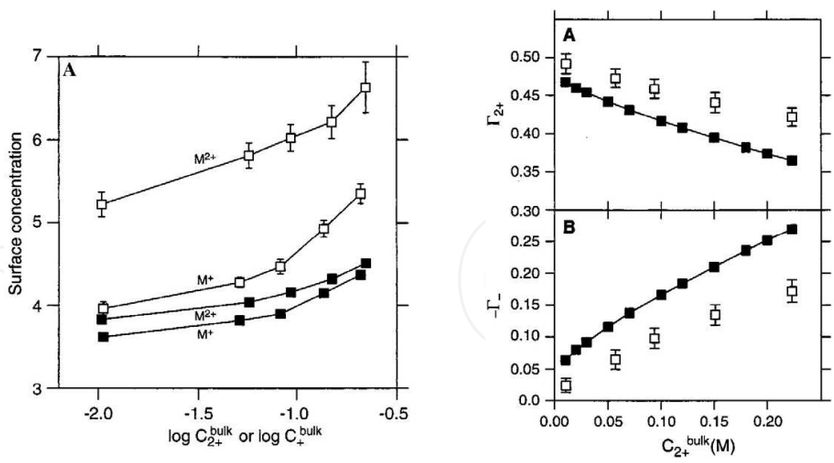

Fig. 2. PB (□) and MC (■) predictions of ion surface concentration (*left*) or preferential interaction coefficients Γ_i (i = -, 2+) (*right*) for 2:1 salt–dsDNA interactions. (Ni et al., 1999)

Nevertheless, emerging interest in phenomena very close to polyion surfaces has spurred development of modified NLPB approaches to account for neglected interactions that become important in high electric fields and large ion concentrations (Grochowski & Trylska, 2008; Tan & Chen, 2009; Wong & Pollack, 2010). Alternatives include PB expressions incorporating excluded volume effects (Bai et al., 2007; Gruziel et al., 2008)

and/or ion correlations (Chu et al., 2008; Ramanathan & Woodbury, 1982), and a hybrid model which explicitly considers ions near the polyelectrolyte surface but uses a continuum description further away (Tan & Chen, 2009).

In summary, CC theory works well at very low salt concentrations ($\lesssim$ 1 mM) and in cases where the details of the ion concentration gradient do not affect behavior but breaks down if these conditions are violated[18]. On the other hand, comparisons of PB calculations to experiments and MC simulations confirm that NLPB approaches effectively and often quantitatively describe systems with up to 1 M univalent salt concentrations (Montoro & Abascal, 1998; Ni et al., 1999). Although differences are evident in ion distributions very close to the polyion, overall determinations of Γ and any closely related thermodynamic phenomena have been shown to be very reliable. At very high salt concentrations (*e.g.*, $\gtrsim$ 2.5 M) or at distances very close to the polyion surface (*i.e.*, $\lesssim$ 3Å for dsDNA), differences between PB and MC calculations become quantitatively significant (Montoro & Abascal, 1998; Ni et al., 1999) at least partially as a result of the greater importance of ion-ion correlations which are present in MC but not in PB.

2.3 Polynucleotide experimental studies

Experimental studies defining polyelectrolyte behavior have predominantly focused on single stranded and double stranded nucleic acid. This section will highlight seminal studies which characterized archetypal polyelectrolyte phenomena: the linear cation NMR relaxation rates in the presence of polynucleotides, the invariance of free solution electrophoretic mobilities with respect to length of high molecular weight NAs, the linear log-salt dependence of thermal denaturation of duplex DNA, and the large salt dependences seen for ligand-nucleic acid interactions.

2.3.1 Small ion NMR of polymeric nucleic acid solutions

^{23}Na NMR has been used to characterize ion-polynucleotide interactions with sonication-derived polydisperse length distributions approximately 700 bp long and various monodisperse DNA samples ranging from 125 – 165 bp in size (Anderson & Record, 1990). ^{23}Na longitudinal and transverse relaxation rates (R_{obs}) are independent of NA sequence and much larger in "salt-free" DNA-containing samples than in otherwise comparable solutions lacking DNA (Braunlin, 1995). The extent of Na^+ association is temperature independent within the 6 – 33 °C range tested, as would be expected if accumulation was due to exclusively electrostatic interactions (Bleam et al., 1983). R_{obs} has been described in terms of a two-state model in which sodium ions are considered either "bound" to the DNA or "free." Bound Na^+ ions rapidly exchange with free Na^+ on the millisecond NMR-timescale and are defined as those ions close enough to DNA that the local electric field gradients perturb $^{23}Na^+$ relaxation rates (R_B). The "free" state includes all other species which possess an average relaxation rate (R_{free}) indistinguishable from R_{obs} for an otherwise comparable DNA-free solution.

[18] For example, Korolev (1998) compared PB and CC predictions with experimental data on the influence of Mg^{2+} on dsDNA thermal denaturation. In this study, CC predicted that Mg^{2+} has a larger nonelectrostatic interaction with ssDNA than dsDNA, the opposite of what was found in PB calculations and in seeming contrast to Raman spectroscopy of DNA which showed only weak differences in the spectra of denatured DNA in the presence *vs* absence of Mg^{2+}.

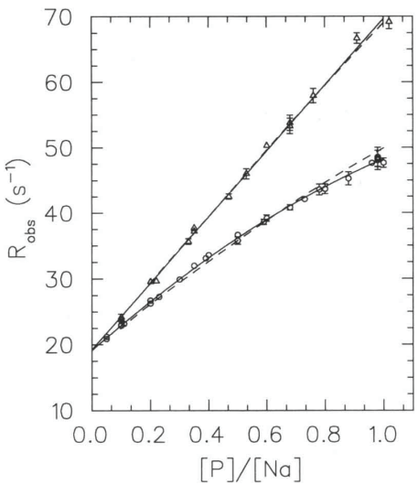

Fig. 3. Two-state analysis of ^{23}Na longitudinal relaxation rates for 160 bp dsDNA (Δ) and 20 bp dsDNA (○) titrated with Na^+. Solid lines are empirical linear and quadratic fits, respectively, and the dashed lines represent the global fit of 20 bp and 160 bp data to $R_{obs} = R_{free} + \alpha C^+_{|Z|}(a)$ [P]/[Na^+], with $\alpha = 28$ and $C^+_{|Z|}(a)$ obtained from GCMC simulations. (Stein et al., 1995)

In general, polymeric DNA has a linear relaxation rate with respect to the concentration ratio of DNA phosphate *vs* total Na^+ within $1 \lesssim$ [Na^+]/[P] $\lesssim 20$ (Stein et al., 1995). This ratio spans DNA phosphate concentrations between 2.5 – 15.1 mM and [Na^+] between 0.003 – 1.3 M. In *Fig.* 3, the y-intercept (*i.e.*, [Na^+] → ∞ as [P]/[Na^+] → 0) in a R_{obs} *vs* [P]/[Na^+] plot corresponds to R_{free} (Bleam et al., 1980). At 1:1 salt conditions (no added salt), $R_{obs} = 69 \pm 1$ s^{-1} is ≈3.6-fold greater than R_{free} (19 ± 1 s^{-1}). By contrast, 20 bp dsDNA has a reduced and significantly nonlinear R_{obs} over the same [P]/[Na^+] range (see Section 3.2.1 and *Fig.* 3). R_{obs} *vs* [P]/[Na^+] data for short and long dsDNA was described with a single fitting parameter, α, weighted by $C^+_{|Z|}(a)$, the axially averaged local Na^+ concentration predicted by GCMC for an appropriately charged cylindrical dsDNA model (*Fig.* 3, *dashed lines*). Interpretations of NMR-measured cation-polyion association data and its comparison to polyelectrolyte theories (*e.g.*, CC, PB, and MC calculations) are reviewed elsewhere (Anderson & Record, 1990; Braunlin, 1995).

2.3.2 Electrophoretic mobility of polymeric nucleic acids

The electrophoretic mobility (μ) of a given nucleic acid depends on the ratio of its total effective charge (q_{eff}) and the frictional coefficient (f) it experiences while moving through the electrophoretic medium,

$$\mu = \frac{q_{eff}}{f}. \tag{17}$$

The independence of electrophoretic mobility on DNA length for long (> 400 bp) DNA strands is well documented in the literature (Olivera et al., 1964; Stellwagen et al., 1997). For example, at 0.01 M NaCl, μ was invariant with DNA length for molecular weights between 1 – 130 MDa (1.5 – 200 kbp) (Olivera et al., 1964). In a series of experiments spanning

0.0001 – 3 M NaCl, poly(styrene sulfonate) strands possessing ~150 – 4500 monomer units exhibited constant μ at fixed [NaCl] with respect to polymer length in capillary electrophoresis or electrophoretic light scattering experiments (Hoagland et al., 1999). Therefore, the independence of μ on DNA length requires that changes in the per monomer effective charge compensate any variation in the per monomer frictional coefficient for long DNAs. *Fig*. 4A demonstrates the length independence of μ for long NAs. Experimental and theoretical studies of polyion electrophoresis phenomena have been reviewed extensively (Allison et al., 2007; Hoagland et al., 1999; Slater et al., 2009; Slater et al., 2002; Viovy, 2000).

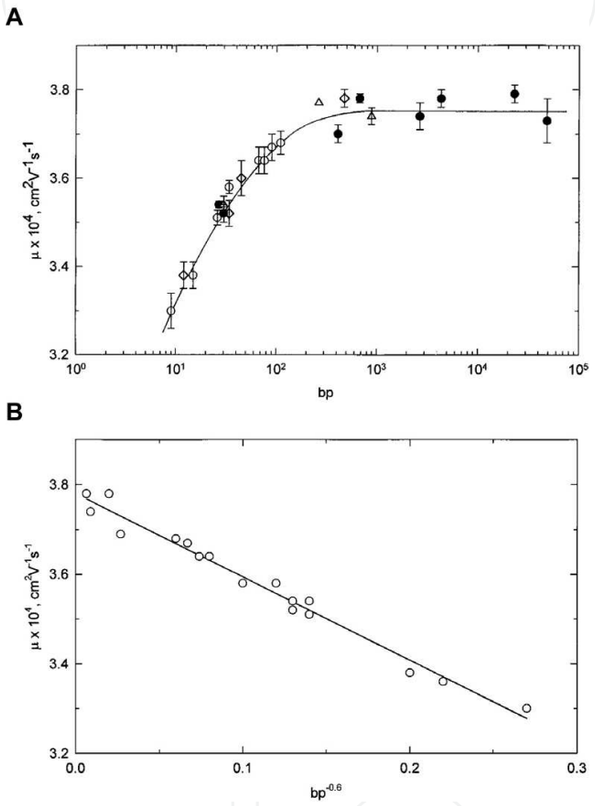

Fig. 4. *A*. dsDNA electrophoretic mobility (μ) measured by capillary electrophoresis of monodisperse DNA (●) and plasmid restriction digest fragments (○, *Msp*I of pBR322; ◇, *HpH*I of pBR322; △, *Taq*I of pUC19) as a logarithmic function of DNA size (in base pairs). The horizontal line indicates the average mobility of long DNA fragments; the curved line is a guide for the eye. *B*. Low molecular weight fragments from (*A*) re-plotted versus the -0.6-power of dsDNA length (in bp). (Stellwagen et al., 1997)

2.2.3 Polymeric melting studies

In general, DNA thermal stability increases with increasing 1:1 salt concentration up to ~1 M. For < 0.2 M salt, the T_m (the midpoint temperature of the thermal transition, where $K_{obs} = 1$) is linear in log[salt]. T_m increases 10—20 °C per decade increase in univalent salt concentration. This behavior is exhibited by both natural and synthetic DNA duplexes and appears to be primarily a coulombic effect. The salt dependence of T_m can be quantitatively interpreted by

$$\frac{\partial T_m}{\partial \ln a_{\pm}} = -\frac{2RT_m^2}{\Delta H_m^o}\Delta\Gamma_u \,, \tag{18}$$

where R is the gas constant and ΔH_m^o is the enthalpic change per nucleotide for the melting transition. Polyelectrolyte Poisson-Boltzmann calculations find that the per-nucleotide $\Delta\Gamma_u$ of nucleic acid transitions has a broad maximum around 0.01 – 0.2 M salt, explaining the relatively constant behavior of $\partial T_m/\partial \ln a_{\pm}$ (Bond et al., 1994; Shkel et al., 2002). NA order-disorder transitions are fully described using experimental ΔH_m^o and T_m values with $\Delta\Gamma$ determined by NLPB on primitive charged cylinders (Fig. 5).

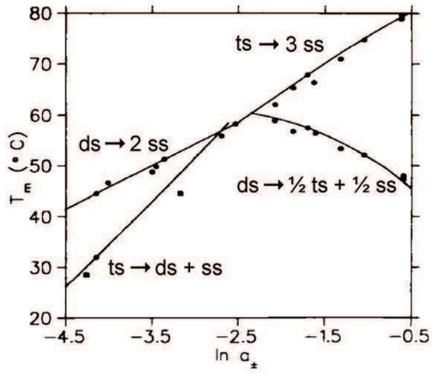

Fig. 5. The dependence of NA melting temperatures, T_m, on the logarithm of NaCl activity ($\ln a_{\pm}$). Symbols denote calorimetric or spectroscopic measurements, while solid lines indicate predictions (eq 18) from NLPB thermodynamic analysis. (Bond et al., 1994)

Researchers have used DNA melting studies to assess oligomer thermodynamics relative to those of polynucleotides. One common approach compared experimental $\partial T_m/\partial \ln a_{\pm}$ values for a given oligonucleotide relative to that predicted for a polymer with the same fractional GC content. As background for later discussion, some of the empirical $\partial T_m/\partial \ln a_{\pm}$ models are surveyed here.

Empirical predictive models for the salt dependence of polymeric nucleic acid denaturation. $\partial T_m/\partial \ln a_{\pm}$ increases linearly with increasing percentages of AT base pairs from 11 – 13 °C at 0%AT to 18 – 20 °C at 100%AT (Blake & Haydock, 1979). The reason behind the GC dependence of $\partial T_m/\partial \ln a_{\pm}$ is not understood, but it is well characterized. Early estimations of $\partial T_m/\partial \ln a_{\pm}$ relied on empirically established linearity between $\partial T_m/\partial \ln a_{\pm}$ and f_{GC}, the fraction of GC base pairs in the DNA duplex, f_{GC} (Blake & Haydock, 1979; Frank-Kamenetskii, 1971). These simple linear relationships are relatively successful, typically predicting $\partial T_m/\partial \ln a_{\pm}$ within ~10% error. However, nearest-neighbor based calculations (Blake et al., 1999; Breslauer, 1986; Delcourt & Blake, 1991) correlate better with experiment and have become the *de facto* standard in many arenas. For example, the salt dependence of thermal denaturation for a d(AT) homopolymer is underestimated by 20% using the method of Frank-Kamenetskii and by 10% using Blake and Haydock's formula but is predicted within 5% of the experimental value by the Blake (1999) nearest neighbor approach. In general, Frank-Kamenetskii, Blake and Haydock, and Blake *et al.* all see approximately a 30% difference in $\partial T_m/\partial \ln a_{\pm}$ for the predicted all-d(AT) and all-d(GC) extremes. These sequence-

dependent methods which predict $\partial T_m/\partial \ln a_\pm$ were mostly developed using long NAs where the thermodynamic consequences of coulombic end effects are expected to be small. Comparisons of the measured oligonucleotide $\partial T_m/\partial \ln a_\pm$ with those predicted by methods described above have led some researchers to suggest that oligomers behave similarly to polymeric NAs (Williams et al., 1989). These comparisons along with other oligonucleotide duplex melting studies will be discussed in greater detail in Section 3.2.5.

2.3.4 Binding of small ligands to polymeric nucleic acids

Polyelectrolyte behavior can also be probed via polyion binding processes with small ligands (including oligocations). Below is a brief summary of some archetypal DNA/RNA-ligand binding reactions described in the literature. Reviews covering a wider array of ligand-nucleic association phenomena are available (Anderson & Record, 1995; Lohman & Mascotti, 1992; Manning, 1978; Record et al., 1978; Record et al., 1998).

Simply speaking, when a cationic ligand with charge Z_L binds to a NA in a solution containing only monovalent salt, counterions are released into the bulk solution providing an entropic driving force for ligand-NA complex formation (Record et al., 1976; Record et al., 1978). Enthalpies observed upon NA binding by oligolysines and polyamines are small and salt-independent, consistent for an entirely entropic driving force (Braunlin et al., 1982; Lohman et al., 1980; Lohman & Mascotti, 1992). The K_{obs} for binding is dependent on the mean ionic activity $a_\pm$ of monovalent salt MX in solution,

$$S_a K_{obs} = \frac{\partial \log K_{obs}}{\partial \log a_\pm} = \Delta(|Z| + 2\Gamma), \tag{19}$$

where "ΔX" is the stoichiometrically-weighted difference between products and reactants (Anderson & Record, 1993; Record et al., 1998). For the process described in eq 1 between DNA (*D*), ligand (*L*), and complex (*LD*), $\Delta X = X_{LD} - X_D - X_L$. It is typically assumed that the binding of the ligand to DNA effectively neutralizes Z_L charges of the DNA (Olmsted et al., 1995; Record et al., 1978).

While eq 19 should be used in general, a highly approximated expression has been found to give good results for an enormous range of systems. Using the limiting law approximations of very low salt, treating the charge of the complex as $|Z_{LD}| = |Z_D| - |Z_L|$, assuming that $\Gamma_{LD} = \Gamma_D$ and that ion release only occurs from the polymer, eq 19 simplifies to

$$\left(\frac{\partial \log K_{obs}}{\partial \log[MX]}\right)_{T,pH}^{LL} = -Z_L(1 + 2\Gamma_D^{LL}) = -Z_L\psi, \tag{20}$$

where $\Gamma_D^{LL} = -\frac{1}{4\xi_D}$ (eq 9) and therefore $\psi = (1 - 0.5\xi_D)$. The original derivation of eq 20 (Record et al., 1976) relied on CC theory (Manning, 1969). Subsequent NLPB evaluations of ψ performed under limiting law conditions yield equivalent results (See Sections 2.2.1 and 2.2.4). dsDNA is thus predicted to have ${}^{ds}\psi = 0.88$ (Record et al., 1976). Similar values of SK_{obs}/Z_L are found regardless of whether the ligand is $Co(NH_3)_6^{3+}$ (Plum & Bloomfield, 1988), polyamines (Braunlin et al., 1982), oligolysines (Lohman et al., 1980; Record et al., 1976), or even proteins such as *lac* repressor (deHaseth et al., 1977) or RNA polymerase (deHaseth et al., 1978) for their nonspecific binding to nonoperator DNA. SK_{obs}/Z_L has

shown variation in some cases, especially when complex formation involves a DNA conformational change. For example, intercalative binding processes typically exhibit reduced SK_{obs}/Z_L ratios, as highlighted by the drug sanguinarine which binds to polymeric dsDNA with SK_{obs}/Z_L ranging between 0.40 – 0.55 (Sen et al., 1996).

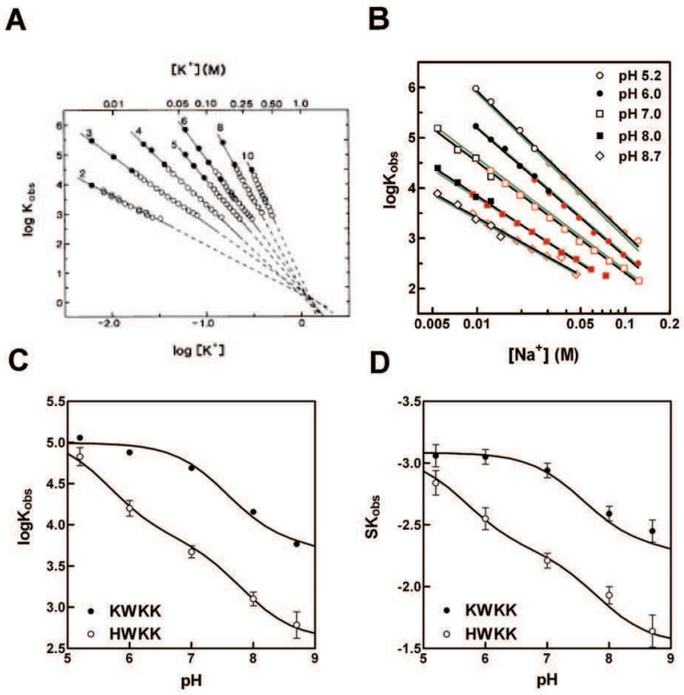

Fig. 6. Cationic peptide binding to polymeric nucleic acids is quantitatively described by limiting-law polyelectrolyte theory. (*A*) Poly(U) binding affinity of oligolysines with charge Z_L = +2 – +10 (as indicated above) exhibits a linear dependence on log[K^+] (Mascotti & Lohman, 1990). (*B*) The salt dependence of poly(U) binding affinity for oligopeptide containing two titratable groups (HWKK) decreases as pH increases from 5.2 – 8.7 (Ballin et al., 2010). (*C*) Poly(U)-XWKK binding constants (where X = histidine (H) or lysine (K)) and their salt dependence (*D*) are accurately predicted via eq 20 by accounting for peptide deprotonation with increasing pH. (Ballin et al., 2010)

The general applicability of eq 20 appears to be extensible to processes involving other polyions and/or ligands which have titratable charges. Extensive binding studies with a series of oligolysine (*Fig.* 6A) and oligoarginine peptides (Z_L = 2 – 10) with various ssDNA and ssRNA NAs found that eq 20 with $^{ss}\psi$ = 0.71 (Mascotti & Lohman, 1990) accounts for the salt dependence of these systems at low salt concentrations at low ligand charge (Z_L = 2 – 4). The full dataset is well fitted if the limiting law expression is augmented to take into account hydration changes upon binding (Mascotti & Lohman, 1990; Mascotti & Lohman, 1993). The linearity of $\log K_{obs}$ *vs* log[salt] has been reported for ligands binding to other polyelectrolytes with varying axial charge densities, ξ, including the polyanionic polysacharride heparin (Mascotti & Lohman, 1995) and polyA•$(polyU)_2$ triple stranded RNA (Record et al., 1976). Eq 20 quantitatively describes binding affinity as a function of salt concentration and pH changes (*Fig.* 6B – D) when ligand deprotonation equilibria are

incorporated into the calculation of Z_L (Ballin et al., 2010; Lohman et al., 1980). Together, these studies show that polyelectrolyte theory effectively describes the electrostatic contributions to binding equilibria and that these contributions are predominantly dictated by gross physical properties such as the net charge and its spatial distribution.

3. Oligonucleotide studies

Residues within the "interior" of a polynucleotide comprise the vast majority of the NA length such that the ends contribute negligibly to the average characteristics of the polyion. Do short NAs whose ends comprise a significant fraction of their oligoion length behave any differently than their polymeric analogs? Below is a brief overview of experimental and theoretical research directly relevant to the thermodynamics of short *vs* long oligoions. This section seeks to address whether there is a coulombic end effect that differentiates the termini of any NA strand from its interior when interacting with other charged species. If such a phenomenon existed, the average per charge coulombic properties of oligoions would vary with Z_D, the total charge of the oligonucleotide until some critical threshold length was attained. The discussion of relevant theoretical work will be followed by a synopsis of experimental efforts to characterize nucleic acid properties that would be sensitive to coulombic end effects: ^{23}Na NMR relaxation rates, electrophoretic mobility, NA melting and NA-ligand interactions. Recent attempts to visualize ion distributions directly by small x-ray scattering will also be discussed.

3.1 Oligoelectrolyte theory

The evolution of oligoelectrolyte theory was similar to that of polyelectrolytes in both chronology and scope. In most cases, existing polyelectrolyte theory was adapted to account for perturbations observed in oligoelectrolyte thermodynamics. For ease of presentation, the oligoelectrolyte theory will be summarized in the following order: 1) counterion condensation theory, 2) Monte Carlo, and then 3) PB. The concepts presented here provide a context for the oligoelectrolyte experimental results presented in Section 3.2.

3.1.1 Counterion condensation and related approaches

In what may have been the first theoretical description of salt effects on an oligoion process, Elson and coworkers modeled thermal denaturation data for a series of intramolecular hairpins by calculating and then summing the discrete pairwise interactions between screened phosphate charges (Elson et al., 1970). The pairwise interactions were determined via the method of Schildkraut and Lifson which uses the linearized PB equation to estimate the screened electrostatic potential as

$$\varphi_{ij} = \frac{z_p e}{\varepsilon r_{ij}} e^{-\kappa r_{ij}} \tag{21}$$

for two phosphate charges i and j separated by a distance r_{ij} with z_p as the effective charge of the phosphates. These summed interactions were used to determine the free energy change of the helix-coil transition and to predict the experimental data using (z_p/ε) as the only fitting factor. Additional details of Elson's study and the subsequent analytical modeling of their data by Record *et al.* (1978) will be discussed further in the context of the experiments that served as their inspiration (See Section 3.2.4).

Ramanathan and Woodbury (1982) considered the BBGKY hierarchy of equations near the PB limit of a uniformly surface-charged cylinder in a continuum dielectric. The authors proved that counterion condensation occurs if ξ surpasses a critical threshold for a charged rod whose length, *L*, is much larger than its radius, *a*, and if this length is also comparable to or larger than the Debye length. The $\xi_{critical}$ is independent of salt concentration if $L \gtrsim \kappa^{-1}$. As the oligoion length decreases, the volume of the condensed layer increases, maintaining the number of ions condensed. When $L < \kappa^{-1}$, $\xi_{critical}$ varied with length and salt concentration (Ramanathan & Woodbury, 1982).

This work inspired Manning and Mohanty (1997) to adapt extended CC theory to finite polyions in the presence of monovalent salt. As discussed in Section 2.2.2, θ represents the average fraction of ions in solution which condense around a polyelectrolyte (*e.g.*, DNA) if $\xi > 1$ for a univalent salt. Manning and Mohanty reported that as the length of the polymer is traversed from the center, θ maintains the idealized (*i.e.*, polymeric) value $\theta = 1 - 1/\xi$ up to approximately κ^{-1} from the terminus. Thereafter, $\theta(s)$ continues to decrease as the end of the polymer is approached by

$$\theta(s) \approx 1 - \frac{\xi_{crit}(s)}{\xi}, \xi > \xi_{crit} \tag{22}$$

where

$$\xi_{crit}(s) = \frac{\ln(\kappa^{-1} / b)}{\ln(s / b)}, L << \kappa^{-1}, \tag{23}$$

and *s* is the contour distance from the terminus of the oligomer (Manning & Mohanty, 1997). In other words, the interior of an oligomer behaves just like that of a polymer for distances more than κ^{-1} from the oligoion terminus. Oligomer (or polymer) regions within κ^{-1} of the terminus will show decreasing extents of ion condensation as the end is approached. The dependence of θ on the spatial proximity to the oligoion terminus reflects a coulombic end effect. For sufficiently short oligoions, a coulombic end effect would also be evidenced as a decrease in θ with decreasing oligomer length *L* since the termini are always within a critical range. Indeed, the CC model predicts that oligoelectrolytes shorter than the Debye length (*i.e.*, $L < \kappa^{-1}$) will exhibit less counterion condensation than a polyion and that, unlike a polyelectrolyte, the threshold for condensation will depend on both the oligoion length and the solution salt concentration (Manning & Mohanty, 1997). In essence, κ^{-1} determines the magnitude and onset of the coulombic end effect expected by CC theory.

Fenley *et al.* (1990) evaluated CC theory predictions for a finite line charge at intermediate salt concentrations (< 0.1 M univalent salt). They found coulombic end effects at low salt which were exhibited as decreased counterion condensation relative to the polymeric limit for regions within approximately κ^{-1} of the line charge termini. To put this into context, a 20 bp dsDNA oligomer has a Debye length of 9.6 Å at 25 °C and 0.1 M univalent salt. According to the Fenley (1990) analysis, a 20 bp dsDNA will exhibit completely polymeric behavior because the DNA oligomer is approximately seven times longer than the Debye length: the predicted average fraction of condensed ions per DNA charge ($\theta = 0.740$) is close to the theoretical limit for a polyelectrolyte ($\theta = 0.764$). If instead of a finite line charge, the polyelectrolyte was modeled as a double-helical array of charges using B-DNA coordinates, the predicted fraction of condensed ions was salt-dependent, in direct conflict with the

experimentally observed salt-invariance of θ. The salt-independence of θ was restored by using an empirical distance-dependent dielectric function near the DNA surface (Fenley et al., 1990). In any case, CC theory predicts that the θ sensitivity to coulombic end effects is insignificantly small under typical experimental conditions[19]. Because θ is directly linked to experimentally measurable thermodynamic quantities, the effective equivalency of θ leads CC theory to predict that there will be no measurable coulombic end effects in NA properties or processes under typical experimentally accessible salt concentrations. These findings will be revisited in Sections 3.1.2 and 3.1.3.

3.1.2 Oligonucleotide Monte Carlo simulations

In one of the first grand canonical Monte Carlo (GCMC) studies of a finite oligoanion, B-DNA (4 – 50 bp) was represented as a right circular cylinder with 3 Å cylindrical end caps in a constant dielectric continuum at low ($a_{\pm}$ = 1.76 mM) monovalent salt (Olmsted et al., 1989). These calculations predicted a significant coulombic end effect: the surface counterion concentration increased linearly with axial position to a distance of approximately 31 Å from the ends. Beyond this distance, the interior showed a polymeric extent of counterion accumulation which was invariant with axial position. Oligomers shorter than ≈24 bp did not attain the maximal surface counterion concentration seen at the interior of polymeric DNA. These findings are in contrast to CC predictions which state that coulombic end effects should only become apparent when the Debye length is *significantly larger* than the oligomer length: even at the low salt concentration (≈2 mM) used in the Olmsted GCMC study, the Debye length κ^{-1} is only ≈2.3-fold greater than the range of the coulombic end effect they observed.

Olmsted's GCMC studies of "primitive" model DNA show that the local cation concentration in the vicinity of the polyion is much smaller at the termini than at positions in the interior (*cf.*, *Fig.* 7A). The result is a roughly inverted parabolic ion distribution which can be approximated as a trapezoid for longer lengths (Olmsted et al., 1989; Olmsted et al., 1991; Olmsted et al., 1995). Increases in NA size beyond a critical length simply increase the length of the plateau region in the interior (*Fig*. 7A-B). If there were no coulombic end effect, the local ion concentration would be relatively invariant over the entire length of the DNA, with little difference at the ends *vs* the center of the polyion.

For B-DNA >10 bp, $\Gamma_{o,u}$ approaches the polymer limit linearly with $1/N$, a relation which holds for the entire 10 – 200 mM univalent salt concentration range considered (Olmsted et al., 1991; Shkel & Record, 2004). In other words, as the DNA strand length is increased, the average counterion accumulation per NA phosphate increases with increasing N and approaches the polymeric limit. The magnitude of the slope for $\Gamma_{o,u}$ *vs* $1/N$ increases with decreasing bulk salt concentration, indicating that larger bulk salt concentrations reduce the length dependence of ion accumulation around DNA (Olmsted et al., 1991; Shkel & Record, 2004). Olmsted *et al.* (1991) used their results to calculate ΔΓ values for DNA thermal denaturation which were in excellent agreement with experimental determinations.

[19] The predicted θ equivalency for oligomers *vs* polymers cannot be used to extrapolate comparisons of Γ_{oligoion} *vs* Γ_{polyion}. Consider, for example, the difference between θ and $\Gamma_{o,u}$. θ represents the fraction of counterions condensed around the polyelectrolyte, whereas $\Gamma_{o,u}$ is representative of all of the counterions in solution.

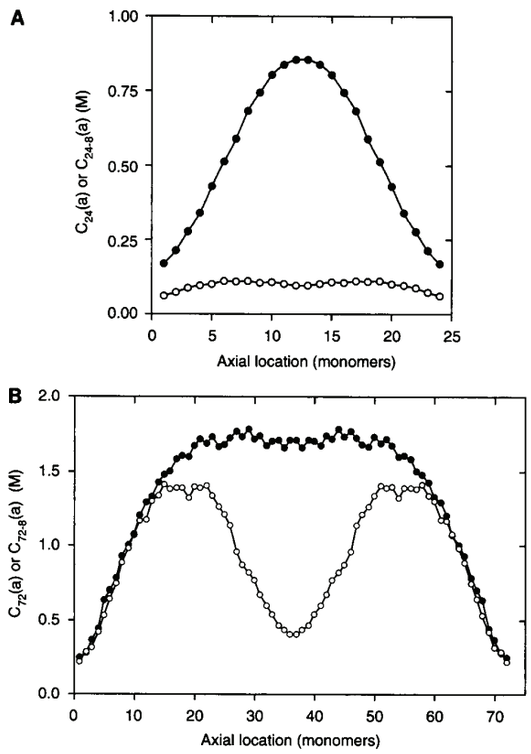

Fig. 7. GCMC predictions of surface counterion concentration $C_{|Z|}(a)$ as a function of axial location (in monomer units) along cylindrical models of uncomplexed and complexed DNA oligomers, the latter with 8 central charges eliminated to simulate binding of a ligand with Z_L = 8+. (A) 24-mer: ●, uncomplexed ($|Z_D|$ = 24); ○, complexed ($|Z_D|$ = 24-8); (B) 72-mer: ●, uncomplexed ($|Z_D|$ = 72); ○, complexed ($|Z_D|$ = 72-8). The axial location of the terminal charge is at position 1. (Olmsted et al., 1995)

Foreshadowing ligand-binding experiments (see Section 3.2.6), Olmsted and coworkers considered the consequences of a +8 cationic ligand binding to short-, intermediate-, and polymeric-length DNA models (Olmsted et al., 1995). Binding was represented by "turning off" 8 charges in the axial center of a given length of DNA. Binding to the center of a 24-mer severely reduced the cation surface concentration around the DNA, whereas binding to the interior of an intermediate-length model DNA effectively created two new "ends" in the interior (*Fig. 7*).

In summary, the GCMC calculations on cylindrical DNA models find that the axial distribution of counterions around the polyion is qualitatively different for short DNA (with its parabolic ion concentration profile and its nonpolymer-like interior) *vs* polymeric DNA (having a trapezoidal ion distributions with a "polymeric" interior). The coulombic end effect stems from the decreasing cation accumulation as the oligomer terminus is approached. Increasing bulk salt concentration decreases the number of terminal residues impacted by the coulombic end effect. The coulombic end effect reduces the overall average per phosphate counterion accumulation around a nucleic acid compared to the polymeric limit. Unlike CC estimations of θ, the GCMC results predict that these effects are significant at experimental salt conditions. The thermodynamics of NA processes such as S_aK_{obs} (eq 19) and $\partial T_m/\partial \ln a_{\pm}$ (eq 18) are direct repercussions of θ and Γ behavior as a function of DNA charge $|Z_D|$.

3.1.3 Oligonucleotide nonlinear Poisson-Boltzmann calculations

Characterization of the coulombic end effect by NLPB. NLPB has also been applied to short nucleic acids. Calculations on DNA lengths between 10—100 bp modeled as right circular cylinders with hemispherical caps exhibited clearly evident coulombic end effects (Allison, 1994). At all monovalent salt concentrations considered (1 – 100 mM), the reduced electric field potential, *y(a)*, at the surface of the DNA cylinder significantly decreases over a ~ 5—6 bp distance as the DNA terminus is approached. Allison (1994) found that to a first approximation, ionic strength and thus Debye length, does not strongly affect the extent of end effects on the polyion electrostatic potential. While the reduced potential *y(r)* is not the same as the surface counterion concentration, Allison's results compare well with those of Olmsted *et al.* (1989, 1991) and Ni *et al.* (1999), probably because counterion concentration is proportional to the exponential of *y(r)* (see eq 14). On the other hand, the large differences seen in *y(a)*, even at high salt concentrations do not correlate well with the predictions of counterion condensation theory which state that the coulombic end effect is very small under these conditions. However, θ is an integral quantity and still may attain polymeric character even if the reduced potential at or near the surface of the DNA is changing with position.

NLPB calculations on a hemispherically-capped cylindrical 80-mer DNA model evaluated the effects of salt concentration and DNA structural parameters on the axial range of the coulombic end effect (Ni et al., 1999). L_{end} is defined as the length from either oligomer terminus where the surface cation concentration reached 95% of the interior concentration. These studies found only a small salt dependence in L_{end} between 0.01 – 0.2 M univalent salt: L_{end} decreased by only 20%over a 20-fold increase in salt concentration. However, L_{end} was much more sensitive to the DNA structural parameters *a* and *b* (See Section 1.2.2). Subsequent NLPB studies discovered that above 0.1 M salt, L_{end} is determined mostly by the polyion cylinder radius, *a*, and charge separation, *b*, and only weakly by κ^{-1} (Shkel & Record, 2004).

NLPB calculations of small ligands binding to oligomers. Several NLPB analyses have considered antibiotic-DNA binding thermodynamics (Chen & Honig, 1997; Misra et al., 1994; Sharp et al., 1995). The interaction of the minor groove-binding antibiotic 4',6-diamidino-2-phenylindole (DAPI) with dsDNA exemplifies the debate on the existence of coulombic end effects. Although the original experimental binding studies of DAPI (a +2 cation) were performed using poly[d(AT)]$_2$ and poly[d(GC)]$_2$ (Wilson et al., 1990), structural data were not available for polymeric DNA. Instead, crystal structure coordinates of a DAPI–12 bp DNA complex were used to construct structurally detailed models of a 12 bp duplex oligomer for NLPB calculations (Misra et al., 1994). The results were then compared to experimental SK_{obs} values for $DAPI^{2+}$ binding to polymeric DNA. They reported that the calculated $DAPI^{2+}$-DNA SK_{obs} was the same for DAPI bound to the 12 bp Dickerson-Drew dodecamer (DDD) sequence (d(CGCGAATTCGCG)$_2$) versus a 57 bp DNA built around a central d(CGCGAATTCGCG)$_2$ binding site, and therefore concluded that there were no end effects. Misra *et al.* stated that the lack of difference is reasonable since DAPI binds at least 13 Å from the terminus of the Dickerson dodecamer and that their results were consistent with previous studies which reported that the coulombic end effect spans a distance of $\approx 0.5\kappa^{-1}$, or approximately 11 Å at 0.02 M salt (Olmsted et al., 1989).

However, Sharp's *et al.* (1995) NLPB studies of DAPI binding to a range of DNA lengths (≈ 8—60 Å or ≈ 2—18 bp) predicted a discernible coulombic end effect for DNA lengths $\lesssim$ 4—5 bp at 0.1 M salt when using a structurally detailed 3-D model for the complex. For dsDNA ≥ 7 bp, the net salt-dependence showed no significant variation over the DNA lengths considered. In other words, Sharp found that DAPI-DNA complex formation

requires oligomer lengths beyond the range where coulombic end effects are readily apparent for divalent ligand binding at 0.1 M salt (Sharp et al., 1995). The Misra (1994) study considered DNA lengths ≥12 bp, and therefore the predicted SK_{obs} of $DAPI^{2+}$-DDD binding should be within error of the experimentally observed SK_{obs} for binding to polymeric dsDNA.

3.1.4 Molecular dynamics simulations

In the last ~15 years, molecular dynamics (MD) simulations have become accepted to such an extent that researchers are using MD for the final stages of structure refinement (Ditzler et al., 2010). Early MD simulations of dsDNA were plagued with problems such as broken base pairing and duplex distortions (Cheatham & Kollman, 2000). However, MD can now make experimentally-consistent predictions such as the spontaneous conversion of an A-DNA duplex into the more thermodynamically stable B-DNA form, ion interactions in the grooves of B-DNA observed in NMR and X-ray studies, and sequence-dependent DNA bending. MD force fields such as AMBER, CHARMM and software packages such as Discovery Studio (Accelrys, Inc.) and GROMOS are now readily accessible[20]. Simulations commonly include full atom representations of macromolecules and many tens of thousands (sometimes millions) of solvent molecules, running simulations on nanosecond timescales or longer. Extreme examples include MD simulations of B-DNA dynamics on the microsecond timescale (Pérez et al., 2007), nucleosome core particle dynamics over a 200 ns interval (Materese et al., 2009), and tRNA entry into the ribosome during decoding (Sanbonmatsu et al., 2005). The extremely high electrostatic fields around NAs require careful consideration of ion and solvent molecules in MD simulations, with as much as 80 – 90% of the computational cost consumed by solvent-solvent interactions (MacKerell & Nilsson, 2008). Some laboratories have attempted to avoid this expense by adopting implicit methods to account for the solvent (Auffinger & Hashem, 2007), though even with these simplifications, large systems still represent a significant challenge. Conformational dynamics or binding processes (with drugs or proteins, for example) are of particular interest. MD methodology development and its applications are intensely active fields of research with reviews being published every year. Here, the basic concepts in MD will be described with salient examples as relevant. Further interest is deferred to an extensive array of available reviews (Auffinger & Hashem, 2007; Ditzler et al., 2010; Egli, 2002; Hashem & Auffinger, 2009; Koehl, 2006; MacKerell & Nilsson, 2008).

MD relies on empirical parameterizations to generate a potential field and then evaluates all atom-atom interactions between the macromolecule and the surrounding water and ions. Potential fields are generally calculated by modeling atoms as Lennard-Jones spheres possessing point charges at their centers, using harmonic spring potential energy functions describe bond lengths and bond angles, and maintaining dihedral angles within a defined torsion profile (Cheatham & Kollman, 2000; Ditzler et al., 2010). Forces acting on each atom are determined from the potential field which dictates the motions of each atom for 1 – 2 femtoseconds. From the new configuration, a new total energy (or free energy, depending on the conditions used) is calculated, and the forces and velocities are calculated again. Everything is dependent on the potential field and continual research strives to improve force field "accuracy" as judged by comparison of MD simulation results to structures

[20] An extensive list of molecular modeling and molecular dynamics software is available at http://www.netsci.org/Resources/Software/Modeling/MMMD/index.html .

predicted by *ab initio* studies or observed experimentally (Cheatham & Kollman, 2000; Hashem & Auffinger, 2009). Often, this has been done by adjustment of the parameters used in the analytical potential field equation of choice. Alternative approaches to defining atomic forces that are particularly important for NA studies include particle mesh Ewald summation (Koehl, 2006) to address the extreme electrostatic fields around the NA and hybrid quantum mechanical/molecular mechanical algorithms (Ditzler et al., 2010), often employed to describe catalytic processes in, for example, ribozymes.

Much of the discussion of ion-nucleic acid interactions in molecular dynamics simulations focuses on ion association or localization, especially in the nucleic acid grooves. Na^+ ion localization at the ApT step in the minor groove of DDD dsDNA is an archetypal example (Young et al., 1997). Since the initial Young *et al.* publication on the "ApT pocket," questions of ion-DNA site-specific binding (Egli, 2002), partial phosphate charge neutralization (Manning, 2003), and the possible repercussions of these phenomena on DNA topology (*e.g.*, bends, twist, groove widening, etc.) continue to be very active fields of research.

However, MD studies which consider ion-NA interactions and the possibility of ion-binding pockets near the NA surface seem to be focused for the most part on NA geometries and radial ion distributions. To our knowledge, very little has been reported on the axial ion distribution which would be most indicative of a coulombic end effect. That said, some studies have considered the extent of phosphate charge neutralization by the surrounding ion atmosphere. One of the earliest examples we could find analyzed the superposition of multiple DNA/counterion structures taken at regular intervals during a 1.5 ns nanosecond simulation of DDD dsDNA in the presence of 22 Na^+ ions (to maintain electroneutrality) and ≈4000 waters (Young et al., 1997). They reported that the "cloud" of counterions around the DNA under no added salt conditions is consistent with Manning's counterion condensation theory, with 76% of the ions condensed around the DNA (Young et al., 1997). A more recent MD simulation on a comparable system (DDD, 22 Na^+ ions, ≈4000 waters, 60 ns simulation) found similar results (Ponomarev et al., 2004). More recently, the net neutralization of DNA charge by core histones and surrounding counterions in the presence of ≈ 50,000 water molecules was considered after a 200 ns MD simulation (Materese et al., 2009). In this study, the authors expected that ≈24% of DNA charge should remain after accounting for the counterion and histone charges within 10 Å of the DNA surface, as anticipated by $\theta = 0.76$ from CC theory. Therefore, approximately 219 counterions were expected near the DNA surface, but only 174 were observed (Materese et al., 2009). Comparisons of radial ion distributions predicted by MD *vs* by PB calculations showed marked differences: the extreme Na^+ accumulation within 3 Å of the nucleosome surface was absent in the PB radial distribution and MD predicted three distinct ionic shells versus only one by PB calculations.

Although molecular dynamics have reproduced some experimental phenomena such as ion localization (Ditzler et al., 2010), current MD force fields generally tend to be insensitive to salt concentration. Simulations of DNA dynamics and structure in solution at nanosecond time-scales have not historically demonstrated significant differences in outcome regardless of whether they are performed in limiting salt, net-neutralizing salt, or even 1 M salt (Cheatham & Kollman, 2000). Of course, this is a serious issue, since differences in salt concentration can dramatically perturb NA structure and processes (*e.g.*, RNA folding and ribozyme function have well known salt concentration sensitivities (Draper et al., 2005)). While MD is considered relatively reliable for protein simulations, reports in 2007 (Auffinger & Hashem, 2007) detailed newly discovered issues with commonly used AMBER force field implementations. For example, some parameterizations resulted in the formation

of ion clusters or aggregates when ≈ 0.25 M KCl or high concentrations of NaCl were added to NA simulations. Hidden errors which were not easily observed in typical < 10 ns simulations led to irreversible DNA backbone torsion angle transitions at long simulation times (> 100 ns) which destroyed DNA structure. Multivalent cations pose a significant challenge for MD simulations and have even been declared outside the applicability of typical force fields (Ditzler et al., 2010). Thus, as summarized in the Supplementary Content for (Krasovska et al., 2006), many researchers choose to run MD simulations with minimal salt to avoid salt-related artifacts. The ion cluster and torsion angle errors described above spurred rapid countermeasures, and MD parameterizations are continually being modified and optimized. Thus, the struggles associated with the strong electrostatic fields around highly charged NAs and multivalent ions may be resolved in time, providing another probe to assess the consequences and causes of coulombic end effects in the properties and processes of NAs.

Summary of theoretical perspectives on end effects. Counterion condensation theory states that the Debye length is the critical factor determining the size and onset of a coulombic end effect and that the significance of end effects on DNA interactions is strongly affected by the salt concentration. At or above 0.1 M univalent salt, the range of the coulombic end effect is predicted to be less than 2—3 bp. Therefore CC theory predicts no significant difference per charge between the coulombic properties of a short oligomer (approximately 5 bp, for example) and a polynucleotide at 0.1 M salt.

NLPB and MC theories predict that the axial profile of the surface counterion concentration is trapezoidal around a polymer and parabolic around a short oligomer. The length of the coulombic end effect is determined by the Debye length at very low salt ($\kappa a << 1$, or millimolar salt concentrations for B-DNA), but DNA radius, a, becomes the characteristic length determining the size of the end effect for high salt (greater than 0.1 M). Between 0.01 – 0.1 M 1:1 salt, the surface potential and counterion axial distribution show coulombic end effects which extend 5—6 bp into the dsDNA and ≈8 bases into the ssDNA interior for long enough oligomers. In both NLPB and MC calculations, preferential interaction coefficients show a linear dependence on the length of the oligomer (*e.g.*, $\Gamma = \Gamma_\infty - \gamma/N$), where both the slope (γ) and the polymeric limit (Γ_∞) are salt dependent and depend on the type (*e.g.*, structural parameters) of the DNA. These computationally derived Γ parameters are equivalent within error to those determined experimentally. Molecular dynamics simulations have found success in predicting ion binding pockets, refining coordinates in experimental structural studies, and correctly predicting some NA conformational changes and ligand interactions. However, MD still has significant difficulty with predicting properties which are sensitive to the extreme electrostatic fields surrounding NAs.

3.2 Oligonucleotide experimental studies

3.2.1 Small ion NMR of nucleic acid solutions

Unlike the linear response of the Na^+ longitudinal relaxation rate, R_{obs}, with increasing $[P]/[Na^+]$ that is observed for polymeric NAs, a short 20 bp dsDNA fragment exhibits a distinctly nonlinear dependence (Section 2.3.1 and *Fig.* 3). As the Na^+ concentration decreased relative to the DNA phosphate concentration, the difference ${}^{160\text{bp}}R_{obs} - {}^{20\text{bp}}R_{obs}$ increased significantly, with the 20 bp fragment always having much less enhancement than the 160-mer at any given $[P]/[Na^+]$ ratio. The divergence of Na^+ relaxation rates between "polymeric" 160 bp DNA and "oligomeric" 20 bp DNA was particularly evident at $[P]/[Na^+] \cong 1$ where ${}^{20\text{bp}}R_{obs} = 47 \pm 1\ s^{-1}$ and ${}^{160\text{bp}}R_{obs} = 69 \pm 1\ s^{-1}$. When compared to $R_{free} = 18.4 \pm 0.4\ s^{-1}$, the 160 bp DNA had almost twice (51 *vs* 29 s^{-1}) the enhancement relative to that seen for the short

oligomer (Stein et al., 1995). Since R_{obs} is indicative of the extent of cation accumulation per phosphate at the DNA surface, these results predict that the average local Na^+ concentration is lower near the surface of the 20-mer than the 160-mer at a given [P]/[Na^+] ratio. These results are consistent with the existence of a significant coulombic end effect: a reduced accumulation of counterions near nucleic acid termini would have a greater impact on the average per-phosphate counterion concentration of shorter nucleic acids since the terminal regions represent a greater proportion of the total oligoion length relative to a polyion.

3.2.2 Structural studies of oligomeric nucleic acids by small angle x-ray scattering

Structural biological applications of small angle x-ray scattering (SAXS) and its variants (*e.g.*, anomalous small-angle x-ray scattering, ASAXS; ultra-small-angle x-ray scattering, USAXS; and small-angle neutron scattering, SANS) have undergone explosive growth in the last decade. While fundamentally a low-resolution technique (typically ranging 10 – 50 Å), SAXS is unfettered by molecular weight constraints or crystallization requirements and can investigate macromolecules in diverse solution conditions with volumes as small as 15 μL and concentrations of ≈20 μM (Putnam et al., 2007). SAXS has been integrated with Monte Carlo, NLPB, molecular dynamics, atomic emission spectroscopy, and NMR applications (Bai et al., 2007; Prabhu, 2005; Rambo & Tainer, 2010). SAXS derives structural information about the population-average of all macromolecule conformations from the pattern of scattered synchrotron radiation. This intensity data is mathematically transformed into its pair distribution, *P(r)*, essentially a histogram of all inter-atomic vectors within the macromolecule. SAXS *P(r)* profiles can be directly calculated from atomic-resolution structures, but the converse is not true. The radius of gyration is directly accessible by SAXS data, thereby providing an estimation of the distribution of mass around its center and thus an indication of the relative size of the macromolecule. The hydrated macromolecular volume can also be obtained for well-folded macromolecules (Putnam et al., 2007; Rambo & Tainer, 2010). The reviews above detail these techniques and available modeling approaches (*e.g.*, rigid-body and refinement modeling) that can be additionally applied.

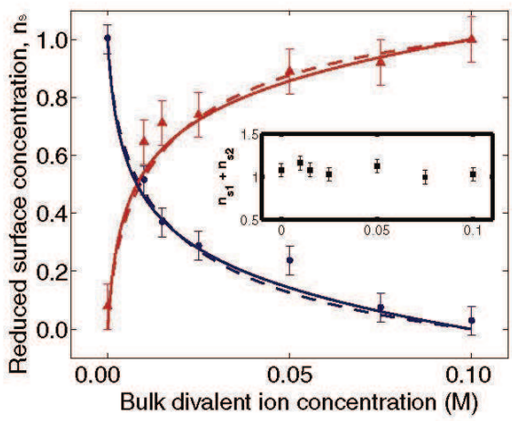

Fig. 8. The measured reduced surface concentrations of Rb^+ (●) and Sr^{2+} (▲) ions are shown as the bulk solution composition is varied. The solid lines represent a global best fit to a Boltzmann distribution of Sr^{2+} relative to Rb^+. The dashed lines represent NLPB calculations accounting for a finite ion radius with a 2 Å distance of closest approach. Inset: the sum of the reduced surface concentrations (■) equals unity within error. (Andresen et al., 2004)

Particularly salient to this review, SAXS has been used to probe NA ion distributions and their perturbation by salt concentration or ion composition changes (Andresen et al., 2004; Andresen et al., 2008; Das et al., 2003; Prabhu, 2005; Rambo & Tainer, 2010). The univalent ion atmosphere around NAs observed by SAXS is remarkably well described by NLPB calculations once finite ion-size adjustments are made (Andresen et al., 2004; Andresen et al., 2008; Das et al., 2003). SAXS studies have corroborated several PB assumptions (*Fig.* 8), including the invariance of equivalently-charged NA-ion distribution profiles and the quantitative validity of eqs 7 and 14 (Andresen et al., 2004; Bai et al., 2007; Das et al., 2003). Similar to PB-MC comparisons discussed previously (*cf.*, Section 2.2.4, *Fig.* 2A), PB calculations tend to overestimate surface cation concentrations near the DNA relative to SAXS-determined values, especially when multivalent cations are present (Andresen et al., 2004; Andresen et al., 2008; Bai et al., 2007; Das et al., 2003).

3.2.3 Oligoelectrolyte capillary electrophoresis

The capillary electrophoresis studies described in Section 2.3.3 compared free solution mobilities (μ) of a range of DNA fragment lengths (27 bp – 48.5 kbp) in tris-acetate-EDTA buffer (Stellwagen et al., 1997). The electrophoretic mobility of oligomers between 10—100 bp decreased monotonically with a –0.6 power-dependence on molecular weight (*Fig.* 4). The increase in μ for smaller DNA fragments with increasing molecular weight are in qualitative agreement with results seen for polylysines (Wilcoxon & Schurr, 1983), small polyphosphates (Grossman & Soane, 1991), and poly(styrene sulfonate) oligoions (Böhme & Scheler, 2007). However, duplexes of $\approx$ 400 bp to 45.8 kbp were independent of molecular weight, consistent with polyelectrolyte behavior (see Section 2.3.3). Does a coulombic end effect contribute to this molecular weight dependence of μ for small oligos?

Mohanty and coworkers (Mohanty & Stellwagen, 1999) derived an expression to describe μ by a series of linearizations of the field and ion transport equations and applied it to the Stellwagen (1997) experimental data. The DNA was modeled as a string of charged beads with a reduced effective charge of (1 - θ) predicted by counterion condensation theory. The condensed fraction of counterions is solely determined by axial charge density ξ (eq 8) at distances greater than the Debye length (*i.e.*, κ^{-1} < 20 Å or < 6 bp at salt concentrations >26 mM used in Stellwagen's experiments). All dsDNA fragments considered exceeded this threshold and thus coulombic end effects are predicted to be negligible. Mohanty's model qualitatively agrees with experiment in that it predicts a plateau in μ for high molecular weight DNA and decreasing with decreasing DNA length. However, the predicted μ decreases too rapidly with decreasing DNA molecular weight in comparison to experiment.

A rigorous continuum hydrodynamic-electrodynamic model describing μ found that the effective charge per base pair decreases with increasing dsDNA length (Allison et al., 2001), indicating that significantly fewer counterions were accumulated per DNA charge for short DNA oligomers than for polymeric DNA. Treating DNA as straight hemispherically capped cylinders predicted electrophoretic mobilities for DNA $\gtrsim$ 60 bp within < 9% of experimental values but overestimated μ for larger fragments (*Fig.* 9). Since the dsDNA persistence length is approximately 50 nm (~ 147 bp), the authors deduced that the increased likelihood of DNA bending for lengths $\gtrsim$ 80 bp may be contributing to the experimentally observed plateau of μ for longer NAs. Unfortunately, the impractical computational time required to sample multiple worm-like chain conformations precluded calculation of an ensemble averaged μ for a population of flexible DNA fragments. However, modeling a series of

singly bent cylinders with the curvature expected for a given length of DNA predicted a μ dependence on length which qualitatively agreed with experiment (*Fig.* 9). Together, these results demonstrate that boundary element modeling (with coulombic end effects) can yield quantitatively better predictions of electrophoretic mobility for short oligomers than a CC approach (without coulombic end effects).

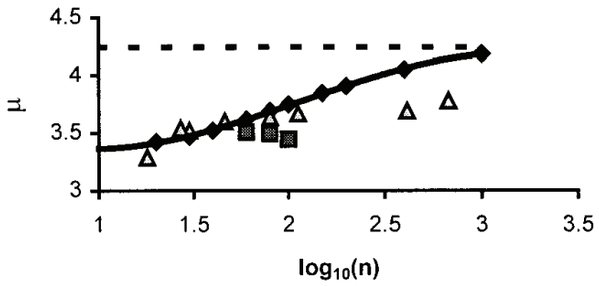

Fig. 9. Comparison of theory and experiment describing the length dependence of electrophoretic mobility, μ. Boundary element calculations modeling dsDNA as straight (◆, *solid curve*) or bent (■) primitive cylinders with hemispherically capped ends possessing phosphates set at half their full charge were compared to experimentally determined μ (Δ) for varying lengths (n, base pairs) of dsDNA oligonucleotides (Stellwagen *et al.*, 1997; *cf. Fig.* 4A above). The dashed line is the idealized mobility of an infinitely long straight rod. (Allison et al., 2001)

Oligomeric nucleic acid processes

Of all oligonucleotide experimental data available relevant to the question of coulombic end effects, thermal denaturation studies probably make up the most plentiful and controversial of results. In the last several years, considerable gains have been made in the characterization and predictions of oligonucleotide stability and its salt dependence. For example, a generalized set of nearest neighbor parameters are now available to describe both polymeric and short nucleic acid hairpins as well as duplex dimer complexes (SantaLucia, 1998). Recent work has generated an empirical function to quantitatively correct for the influence of divalent cations on the thermal denaturation of dsDNA oligomers (Owczarzy et al., 2008). The theoretical work of Olmsted *et al.* (1991) and Shkel & Record (2004) employ coulombic end effects to accurately describe several of the denaturation studies known at the time. However, observed and theoretical thermodynamic descriptions of NA melting led some to believe that coulombic end effects were not necessary to describe oligonucleotide melting. This brief synopsis describes some of the experimental results which seeded this controversy and concludes with a summary of oligonucleotide-ligand binding studies which more readily detected the deviation of oligonucleotide behavior from the polyelectrolyte ideal.

3.2.4 Conformational changes: denaturation of hairpin double helices (one folded strand)

In one of the first systematic melting studies of nucleic acid oligomers, Elson and coworkers investigated the thermodynamics of melting hairpin double helices formed by the intramolecular association of series of d(AT) oligomers possessing between 18 and 44 phosphate charges (Elson et al., 1970). The melting temperature T_m and its salt dependence $\partial T_m/\partial \log[\text{salt}]$ for these hairpins decreased sharply from typical polymeric values with

decreasing $|Z|$, the number of oligonucleotide phosphate charges (*Fig.* 10). They used *a priori* computations based on the summation of discrete pairwise interactions of the screened DNA phosphate charges to describe their hairpin denaturation experiments (see Section 3.1.1) and found that a single value was sufficient to model all oligomer melting transitions at all salt concentrations studied. However, it was necessary to count the interactions between charges

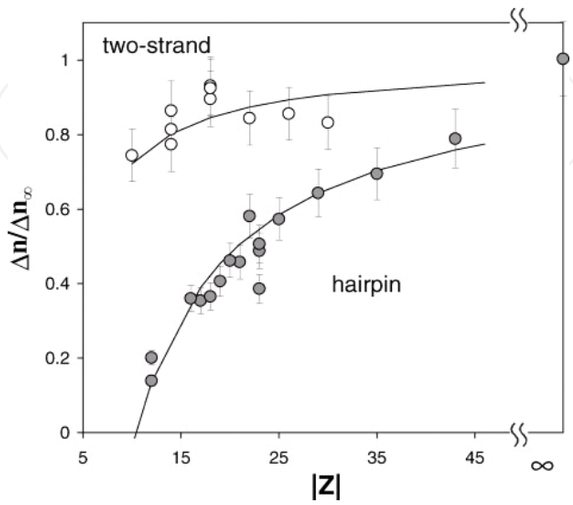

Fig. 10. The salt dependence of thermal denaturation ($ST_m = \partial T_m/\partial \ln[salt]$) as a function of NA charge $|Z|$ for (○) two-stranded and (●) hairpin NAs (including the Elson (1970) oligomers) plotted in terms of the net change in per-phosphate ion accumulation (Δn) upon thermal denaturation relative to Δn_u in the infinite polymer limit (Δn_∞). Solid lines trace $\frac{\Delta n_u}{\Delta n_{u,\infty}} = 1 - \frac{\gamma_{\text{end}}}{|Z|}$, where γ_{end} is the NLPB- determined coulombic end effect parameter quantifying the reduced fraction of ion accumulation near oligoion termini. These results relate to experiment by $\frac{ST_m}{ST_{m,\infty}} = \frac{\Delta n_u}{\Delta n_{u,\infty}} \frac{|Z|}{N_n - X} = \frac{|Z| - \gamma_{\text{end}}}{N_n - X}$, with N_n as the number of nucleotides in the native conformation and X, the number of nucleotides not contributing to the reaction enthalpy (*i.e.*, N_{loop} nucleotides in a hairpin loop). (Shkel & Record, Jr., 2004)

NA native state	γ_{end}	Valid regime	$(N_n - X)$
two-stranded duplex	2.8	$\|Z\| \geq 8$	$\|Z\|$
single-loop hairpin	10.4	$\|Z\| \geq 13$	$\|Z\| - N_h - 1$
double-loop hairpin	10.4	$\|Z\| \geq 13$	$\|Z\| - N_h + 1$

both in the helical and nonhelical segments of the hairpins to accurately model the breadth of the melting transitions. Record *et al.* (1978) developed an approximate analytical treatment of these data, using an end effect parameter in a CC-like theory to predict the observed $1/|Z|$ dependence of the $\partial T_m/\partial \log[salt]$ of hairpin melting. The methodology developed by Record and coworkers (1978) did not consider the nonhelical hairpin segments nor require any details of DNA structure other than the DNA axial charge separation b, yet fit the hairpin data quite well. A subsequent generalization of this approach (Olmsted et al., 1991) used GCMC simulations (*cf.*, Section 3.2.2) to predict with

good accuracy the $\Delta\Gamma$ of ds $\rightarrow$ ss conversion for the Elson *et al.* (1970) hairpin studies. This same methodology, which predicts sizable coulombic end effects for short oligomers, describes hairpin denaturation, the melting transitions of dumbbell-shaped double-hairpins (Erie et al., 1987) and several of the two-stranded NA dimer denaturation studies known at the time. Shkel & Record (2004) revisited these experimental systems using NLPB calculations to develop a parameterized formula predicting $\partial T_m/\partial\log[\text{salt}]$ via consideration of the average ion accumulation near ssDNA and dsDNA termini relative to the polymeric limit (*Fig.* 10).

3.2.5 Conformational changes: two-stranded duplex ("dimer") denaturation

Some of the earlier spectroscopic, thermodynamic, and kinetic melting studies of short oligonucleotide two-stranded duplexes reported that the $\partial T_m/\partial\log[\text{salt}]$ in these systems was closer to that expected for polymeric nucleic acids with similar GC content than to analogous values seen in the hairpin melting studies described above. For example, the experimentally measured $\partial T_m/\partial\log[\text{salt}]$ for d(GCATGC) dsDNA ranged between 11 – 15 °C depending on strand concentration (Williams et al., 1989), which was consistent with a predicted $\partial T_m/\partial\log[\text{salt}]$ of 13.6 – 15.5 °C based on formulae developed to describe polymeric denaturation (Blake & Haydock, 1979; Frank-Kamenetskii, 1971). ^{1}H-NMR studies (Braunlin & Bloomfield, 1991) describing thermodynamic and kinetic salt effects on strand association for d(GGAATTCC) found that 0.13 ± 0.02 Na^+ ions are released per phosphate upon duplex dissociation, which compares well with the estimated 0.17 ions released per phosphate for polymeric DNA (Record et al., 1976). In both cases, the authors concluded that their oligonucleotide results were the same within uncertainty as those expected for the corresponding polymeric systems.

A comprehensive data review (SantaLucia, 1998) summarized both polymeric and oligomeric results across seven studies of DNA and RNA stability, including the Braunlin and Williams oligomers mentioned above. All experimental results were presented in a common format, thereby allowing direct comparison of free energies and their salt dependences. Experimental measurements of 26 NAs possessing 4 – 16 nucleotides had an average $\partial\Delta G°_{37}/\partial\ln[\text{salt}]$= - (0.057 ± 0.017) *$|Z_D|$ kcal/mol between 0.1 – 0.3 M NaCl. In other words, the sensitivity of NA thermal stability to salt concentration was found to be linearly proportional to the number of phosphates in the duplex, $|Z_D|$ (SantaLucia et al., 1996). Global analysis of three polymeric datasets (30 data points) yields an average $\partial\Delta G°_{37}/\partial\ln[\text{salt}]$= -(0.175 ± 0.034) kcal/mol, independent of polymer length (SantaLucia, 1998). The larger $\partial\Delta G°_{37}/\partial\ln[\text{salt}]$ for polynucleotide denaturation *vs* oligonucleotide melting in conjunction with the length dependence of $\partial\Delta G°_{37}/\partial\ln[\text{salt}]$ for oligomers but not for polymers, are consistent with a coulombic end effect.

The melting thermodynamics of two-stranded oligomers appear polymeric due to a cancellation of effects: the duplex initial state denatures into two separate single strands, each with half the number of charges of the duplex. The net charge of the reactants does not change in denaturation studies ($\Delta Z = 0$) and thus[21] $\partial\Delta G°/\partial\ln[\text{salt}] = -2RT\Delta\Gamma$ by eq 19. Although the length dependence of Γ for the native and denatured states of two-stranded

[21] Substitution of $-\Delta G°/RT = \ln K_{obs}$ and $\ln[Na^+] \approx \ln a_{\pm}$ into eq 19 gives $\dfrac{\partial\Delta G^o}{\partial\ln[Na^+]} = -RT\Delta(|Z|+2\Gamma)$.

duplexes are significant, $\Delta\Gamma$ for the melting transition is relatively constant across a wide range of oligomer lengths. As a result, the dramatic coulombic end effects evident in NMR Na^+ relaxation experiments and hairpin thermal denaturation studies are not seen in two-strand duplex melting processes. Comparisons of oligonucleotide melting behavior of hairpins and dimer duplexes with calculations of $\Delta\Gamma$ are described in greater detail by Shkel and Record (2004). Perhaps most telling, theories which include coulombic end effects (Olmsted et al., 1991; Shkel & Record, 2004) accurately account for the melting transitions of NA hairpins and short two-stranded duplex DNA within experimental error, including d(GCATGC) (Braunlin & Bloomfield, 1991) and d(GGAATTCC) (Williams et al., 1989).

3.2.6 Oligonucleotide ligand binding

Zhang et al. (1996) performed possibly the first cationic oligopeptide-oligonucleotide binding studies to assess the difference of Z_L = 8+ peptide (KWK_6) binding to $dT(pdT)_{10}$ and poly(dT) ($dT(pdT)_{169}$). They reported that the binding affinity for KWK_6 binding to poly(dT) versus $dT(pdT)_{10}$ was about 13 times greater at 0.2 M Na^+ and 76-fold greater at 0.1 M Na^+.

The salt dependence of the equilibrium binding constant at 0.2 M Na^+ was – 6.5 ± 0.2 for poly(dT) but – 3.5 ± 0.1 for $dT(pdT)_{10}$. Poly(dT) had an extrapolated $\log K_{obs}$ at 1 M salt of - 0.6, indicating that ligand binding is unfavorable at such a high salt concentration and, more importantly, that binding is dominated by the entropic driving force of cation release characteristic of polyelectrolytes (see Section 2.3.4). $dT(pdT)_{10}$, on the other hand, has a 1 M Na^+ $\log K_{obs}$ of 0.7, still indicating that most of the poly(dT)-KWK_6 stabilization is from cation release, but with much less net thermodynamic counterion release upon complex formation. The large differences in S_aK_{obs} seen for long *vs* short nucleic acids to oligopeptides are consistent with PB (Zhang et al., 1996) and GCMC predictions (Olmsted et al., 1995). The greatly reduced salt dependence of binding is consistent with a significant change in the binding process $\Delta\Gamma$ for $dT(pdT)_{10}$ *vs* polydT (eq 19). These results conflict with the expectations of CC-based theories which maintain that little or no difference in S_aK_{obs} should be evidenced at these salt concentrations (see Section 3.1.1).

Subsequent studies of KWK_6 binding to intermediate lengths of $dT(pdT)_{|Z_D|}$, where $|Z_D|$ is the number of phosphate charges on the DNA, were later performed (Zhang et al., 1999) to define the transition from oligomeric binding of $dT(pdT)_{10}$ to polymeric binding of poly(dT). $\text{Log}K_{obs}$ and $|S_aK_{obs}|$ at 0.1 M Na^+ monotonically increased as length increased through the intermediate range $15 \leq |Z_D| \leq 69$, with values which were bracketed between the corresponding measures observed for $dT(pdT)_{10}$ and polydT. Zhang and coworkers found that S_aK_{obs} and $\Delta G°$ were inversely proportional to the number of binding sites (*Fig.* 11). Using a two-state model , they estimated that "end sites" spanning ≈10 phosphates had reduced ion accumulation relative to that expected for a ssDNA polyelectrolyte (Zhang et al., 1999). With collection of additional ssDNA-KWK_6 binding data (Ballin et al., 2004), Shkel and coworkers derived a parametric expression that quantitatively describes the full scope of nonspecific ligand-ssDNA binding studies they considered. Nonlinear least squares analysis of the experimental data indicated that coulombic end effects have a characteristic length affecting 9.0 ± 0.8 residues from each ssDNA terminus and 12 ± 1 residues from each end of dsDNA (Shkel et al., 2006). The minimum DNA length required to exhibit polymeric binding affinity and SK_{obs} for a ligand with Z_L charges is $|Z_D| = Z_L + 2N_e$ where N_e = 9.0 ± 0.8

for ssDNA and N_e = 12 ± 1 for dsDNA. In other words, Mg^{2+} with Z_L = +2 would bind 27 bp dsDNA with polymeric affinity since polymeric binding is predicted for $|Z_D| > 2*12 + 2 = 26$.

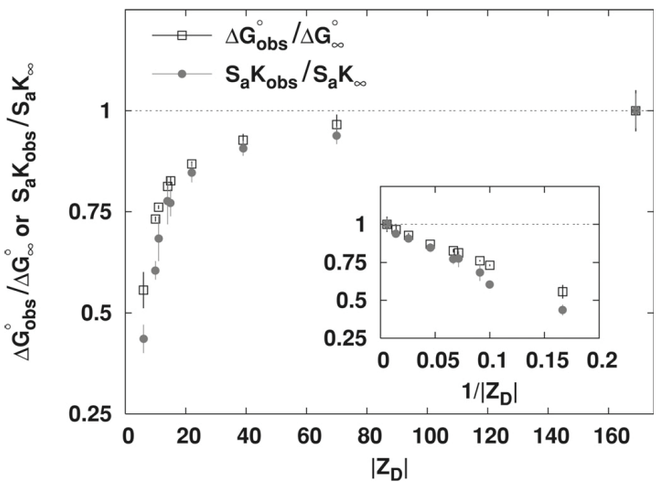

Fig. 11. $\Delta G°_{obs}$ and S_aK_{obs} for KWK_6 (Z_L = 8+) binding to ssDNA depends on DNA charge, $|Z_D|$. Values of $\Delta G°_{obs}$ at 0.1 M Na+ (□) and S_aK_{obs} (●), normalized by the corresponding quantities for binding of KWK_6 to poly(dT), are plotted against the number of DNA charges, $|Z_D|$. The inset plots the same data versus $1/|Z_D|$. (Ballin et al., 2004)

Conclusions

The experimental and theoretical results strongly support the existence of a coulombic end effect on processes involving oligonucleotides or which interact with the termini of long NAs. All experimental systems amenable to easy detection of putative coulombic end effects show such effects. Models incorporating coulombic end effects also accurately predict experimentally observed behavior for systems where end effects are expected to cancel out or be insignificantly small relative to larger effects. However, theories which neglect coulombic end effects and hence predict no difference between short *vs* long oligoelectrolytes fail to explain these phenomena and are therefore called into question. Nevertheless, theoretical systems exhibiting the greatest success in providing a unified explanation of nucleic acid properties from short to polymeric lengths account for coulombic end effects and their consequences, consideration of which is crucial for the understanding of nucleic acid phenomena in biochemistry and biotechnology.

4. Future directions

The four decades since the first reports of CC theory have witnessed tremendous advancements. Computational methods such as MC and NLPB accurately describe many polyelectrolyte thermodynamic signatures and their transitions into oligoelectrolyte behavior. Predictions are generally reliable for processes occurring at intermediate (*e.g.*, nonspecific binding events, ion distribution functions > 5 – 6 Å from the NA surface, etc.) or very far distances from the polyion (*e.g.*, colligative properties such as Donnan equilibria). These successes have encouraged researchers to tackle increasingly more difficult problems. In particular, we expect to see a growing interest in understanding processes which occur

very close to the NA surface. Success in this arena will require significant improvements in the theoretical description of coulombic phenomena in extremely high field gradients, including ion-ion and ion-solvent interactions, polarizability, etc. How are these factors influenced by bent or kinked NA structures? Efficient integration of large-domain macromolecular dynamics (reptation models are of particular import for theories treating NA electrophoresis), intermediate-timescale conformational changes in RNA subdomains (essential for understanding catalytic RNA mechanisms), and a better understanding of the role of water in these processes (a universal challenge) will also become important. Of course, the excitement around SAXS and other atomic-level visualization techniques will likely continue. SAXS investigations of inter-helix DNA interactions in the presence of high-valence salts represent an active area of research. A study of the axial distribution of ions could provide enticing insights into processes involving siRNA, tRNA, and NA-drug interactions which could be compared to computational predictions.

The recent derivations of analytical solutions to the PB equation at all physiologically relevant salt concentrations may provide a viable alternative to the primitive parametric Hook's Law/Lennard-Jones potential fields used in molecular dynamics simulations. Despite their limiting assumptions, PB calculations have an enormous and growing body of evidence (SAXS, experimentally validated predictions of NA stability and its response to solution conditions, RNA folding thermodynamics, etc.) contending that PB is an effective tool for predicting electrostatic phenomena. Recent work has shown that expansion-series solutions to the PB equation yield electrostatic energy predictions that are within 2% of unapproximated calculations. The authors would like to see implementation of these simplified yet still quantitatively accurate electrostatic formulae into a MD algorithm. Such efforts could catalyze needed characterization and predictive model development describing the ***nonelectrostatic*** contributions to biomolecular processes.

5. Acknowledgement

The authors are grateful for stimulating discussions with Drs. M. Thomas Record, Jr., Charles F. Anderson, and Irina A. Shkel throughout the development of this work and would like to thank Dr. Irina A. Shkel for her thoughtful critique and helpful comments on a draft of this chapter.

6. References

Allison, S. A. (1994). End effects in electrostatic potentials of cylinders: models for DNA fragments. *J. Phys. Chem.* Vol. 98, No. 46, pp. 12091-12096, ISSN 0022-3654.

Allison, S. A.; Chen, C. & Stigter, D. (2001). The length dependence of translational diffusion, free solution electrophoretic mobility, and electrophoretic tether force of rigid rod-like model duplex DNA. *Biophys. J.* Vol. 81, No. 5, pp. 2558-2568, ISSN 0006-3495.

Allison, S. A.; Pei, H. & Xin, Y. (2007). Modeling the free solution and gel electrophoresis of biopolymers: the bead array-effective medium model. *Biopolymers* Vol. 87, No. 2-3, pp. 102-114, ISSN 1097-0282.

Anderson, C. F. & Record, M. T., Jr. (1980). The relationship between the Poisson-Boltzmann model and the condensation hypothesis: an analysis based on the low salt form of the Donnan coefficient. *Biophys. Chem.* Vol. 11, No. 3-4, pp. 353-360, ISSN 0301-4622.

Anderson, C. F. & Record, M. T., Jr. (1982). Polyelectrolyte theories and their applications to DNA. *Annu. Rev. Phys. Chem.* Vol. 33, No. 1, pp. 191-222, ISSN 0066-426X.

Anderson, C. F. & Record, M. T., Jr. (1983).The thermodynamic effects of polyelectrolyte-electrolyte interactions. In: *Structure and Dynamics: Nucleic Acids and Proteins,* E. Clementi & R. H. Sarma, (Ed.), Adenine Press, ISBN 0-940030-04-7, NY NY.

Anderson, C. F. & Record, M. T., Jr. (1990). Ion distributions around DNA and other cylindrical polyions: theoretical descriptions and physical implications. *Annu. Rev. Biophys. Biophys. Chem.* Vol. 19, No. 1, pp. 423-463, ISSN 0883-9182.

Anderson, C. F. & Record, M. T., Jr. (1993). Salt dependence of oligoion-polyion binding: a thermodynamic description based on preferential interaction coefficients. *J. Phys. Chem.* Vol. 97, No. 27, pp. 7116-7126, ISSN 0022-3654.

Anderson, C. F. & Record, M. T., Jr. (1995). Salt-nucleic acid interactions. *Annu. Rev. Phys. Chem.* Vol. 46, No. 1, pp. 657-700, ISSN 0066-426X.

Andresen, K.; Das, R.; Park, H. Y.; Smith, H.; Kwok, L. W.; Lamb, J. S.; Kirkland, E. J.; Herschlag, D.; Finkelstein, K. D. & Pollack, L. (2004). Spatial distribution of competing ions around DNA in solution. *Phys. Rev. Lett.* Vol. 93, No. 24, pg. 248103, ISSN 0031-9007.

Andresen, K.; Qiu, X.; Pabit, S. A.; Lamb, J. S.; Park, H. Y.; Kwok, L. W. & Pollack, L. (2008). Mono- and trivalent ions around DNA: a small-angle scattering study of competition and interactions. *Biophys. J.* Vol. 95, No. 1, pp. 287-295, ISSN 0006-3495.

Auffinger, P. & Hashem, Y. (2007). Nucleic acid solvation: from outside to insight. *Curr. Opin. Struct. Biol.* Vol. 17, No. 3, pp. 325-333, ISSN 0959-440X.

Bai, Y.; Greenfeld, M.; Travers, K. J.; Chu, V. B.; Lipfert, J.; Doniach, S. & Herschlag, D. (2007). Quantitative and comprehensive decomposition of the ion atmosphere around nucleic acids. *J. Am. Chem. Soc.* Vol. 129, No. 48, pp. 14981-14988, ISSN 0002-7863.

Ballin, J. D.; Prevas, J. P.; Ross, C. R.; Toth, E. A.; Wilson, G. M. & Record, M. T., Jr. (2010). Contributions of the histidine side chain and the N-terminal α-amino group to the binding thermodynamics of oligopeptides to nucleic acids as a function of pH. *Biochemistry* Vol. 49, No. 9, pp. 2018-2030, ISSN 0006-2960.

Ballin, J. D.; Shkel, I. A. & Record, M. T., Jr. (2004). Interactions of the KWK_6 cationic peptide with short nucleic acid oligomers: demonstration of large coulombic end effects on binding at 0.1-0.2 M salt. *Nucleic Acids Res.* Vol. 32, No. 11, pp. 3271-3281, ISSN 0305-1048.

Blake, R. D.; Bizzaro, J. W.; Blake, J. D.; Day, G. R.; Delcourt, S. G.; Knowles, J.; Marx, K. A. & SantaLucia, J. J. (1999). Statistical mechanical simulation of polymeric DNA melting with MELTSIM. *Bioinformatics* Vol. 15, No. 5, pp. 370-375, ISSN 1367-4803.

Blake, R. D. & Haydock, P. V. (1979). Effect of sodium ion on the high-resolution melting of lambda DNA. *Biopolymers* Vol. 18, No. 12, pp. 3089-3109, ISSN 1097-0282.

Bleam, M. L.; Anderson, C. F. & Record, M. T., Jr. (1980). Relative binding affinities of monovalent cations for double-stranded DNA. *Proc. Natl. Acad. Sci. USA* Vol. 77, No. 6, pp. 3085-3089, ISSN 0027-8424.

Bleam, M. L.; Anderson, C. F. & Record, M. T., Jr. (1983). Sodium-23 nuclear magnetic resonance studies of cation-deoxyribonucleic acid interactions. *Biochemistry* Vol. 22, No. 23, pp. 5418-5425, ISSN 0006-2960.

Böhme, U. & Scheler, U. (2007). Hydrodynamic size and electrophoretic mobility of poly(styrene sulfonate) versus molecular weight. *Macromol. Chem. Phys.* Vol. 208, No. 19-20, pp. 2254-2257, ISSN 1521-3935.

Bond, J. P.; Anderson, C. F. & Record, M. T., Jr. (1994). Conformational transitions of duplex and triplex nucleic acid helices: thermodynamic analysis of effects of salt concentration on stability using preferential interaction coefficients. *Biophys. J.* Vol. 67, No. 2, pp. 825-836, ISSN 0006-3495.

Braunlin, W. H. (1995).NMR studies of cation binding environments on nucleic acids. In: *Advances in Biophysical Chemistry,* C. A. Bush, (Ed.), Jai Press, Inc, ISBN 1-55938-978-8, Greenwich CT.

Braunlin, W. H. & Bloomfield, V. A. (1991). Proton NMR study of the base-pairing reactions of d(GGAATTCC): salt effects on the equilibria and kinetics of strand association. *Biochemistry* Vol. 30, No. 3, pp. 754-758, ISSN 0006-2960.

Braunlin, W. H.; Strick, T. J. & Record, M. T., Jr. (1982). Equilibrium dialysis studies of polyamine binding to DNA. *Biopolymers* Vol. 21, No. 7, pp. 1301-1314, ISSN 0006-3525.

Breslauer, K. J. (1986).*Thermodynamic Data for Biochemistry and Biotechnology*. H.-J. Hinz, (Ed.), pp. 402-427, Springer-Verlag, ISBN 0387163689, New York NY.

Cheatham, T. E., III & Kollman, P. A. (2000). Molecular dynamics simulation of nucleic acids. *Annu. Rev. Phys. Chem.* Vol. 51, No. 1, pp. 435-471, ISSN 0066-426X.

Chen, S. W. W. & Honig, B. (1997). Monovalent and divalent salt effects on electrostatic free energies defined by the nonlinear Poisson-Boltzmann equation: Application to DNA binding reactions. *J. Phys. Chem. B* Vol. 101, No. 44, pp. 9113-9118, ISSN 1089-5647.

Chu, V. B.; Bai, Y.; Lipfert, J.; Herschlag, D. & Doniach, S. (2008). A repulsive field: advances in the electrostatics of the ion atmosphere. *Curr. Opin. Chem. Biol.* Vol. 12, No. 6, pp. 619-625, ISSN 1367-5931.

Das, R.; Mills, T. T.; Kwok, L. W.; Maskel, G. S.; Millett, I. S.; Doniach, S.; Finkelstein, K. D.; Herschlag, D. & Pollack, L. (2003). Counterion distribution around DNA probed by solution x-ray scattering. *Phys. Rev. Lett.* Vol. 90, No. 18, pg. 188103, ISSN 0031-9007.

deHaseth, P. L.; Lohman, T. M.; Burgess, R. R. & Record, M. T., Jr. (1978). Nonspecific interactions of *Escherichia coli* RNA polymerase with native and denatured DNA: differences in the binding behavior of core and holoenzyme. *Biochemistry* Vol. 17, No. 9, pp. 1612-1622, ISSN 0006-2960.

deHaseth, P. L.; Lohman, T. M. & Record, M. T., Jr. (1977). Nonspecific interaction of lac repressor with DNA: an association reaction driven by counterion release. *Biochemistry* Vol. 16, No. 22, pp. 4783-4790, ISSN 0006-2960.

Delcourt, S. G. & Blake, R. D. (1991). Stacking energies in DNA. *J. Biol. Chem.* Vol. 266, No. 23, pp. 15160-15169, ISSN 0021-9258.

Ditzler, M. A.; Otyepka, M.; Sponer, J. & Walter, N. G. (2010). Molecular dynamics and quantum mechanics of RNA: conformational and chemical change we can believe in. *Acc. Chem. Res.* Vol. 43, No. 1, pp. 40-47, ISSN 0001-4842.

Draper, D. E.; Grilley, D. & Soto, A. M. (2005). Ions and RNA folding. *Annu. Rev. Biophys. Biomol. Struct.* Vol. 34, pp. 221-243, ISSN 1056-8700.

Draper, D. E. (2008). RNA folding: thermodynamic and molecular descriptions of the roles of ions. *Biophys. J.* Vol. 95, No. 12, pp. 5489-5495, ISSN 0006-3495.

Egli, M. (2002). DNA-cation interactions: quo vadis? *Chem. Biol.* Vol. 9, No. 3, pp. 277-286, ISSN 1074-5521.

Elson, E. L.; Scheffler, I. E. & Baldwin, R. L. (1970). Helix formation by d(TA) oligomers: III. Electrostatic effects. *J. Mol. Biol.* Vol. 54, No. 3, pp. 401-415, ISSN 0022-2836.

Erie, D.; Sinha, N.; Olson, W.; Jones, R. & Breslauer, K. (1987). A dumbbell-shaped, double-hairpin structure of DNA: a thermodynamic investigation. *Biochemistry* Vol. 26, No. 22, pp. 7150-7159, ISSN 0006-2960.

Fenley, M. O.; Harris, R. C.; Jayaram, B. & Boschitsch, A. H. (2010). Revisiting the association of cationic groove-binding drugs to DNA using a Poisson-Boltzmann approach. *Biophys. J.* Vol. 99, No. 3, pp. 879-886, ISSN 0006-3495.

Fenley, M. O.; Manning, G. S. & Olson, W. K. (1990). Approach to the limit of counterion condensation. *Biopolymers* Vol. 30, No. 13-14, pp. 1191-1203, ISSN 1097-0282.

Fixman, M. (1979). The Poisson--Boltzmann equation and its application to polyelectrolytes. *J. Chem. Phys.* Vol. 70, No. 11, pp. 4995-5005, ISSN 0021-9606.

Fogolari, F.; Brigo, A. & Molinari, H. (2002). The Poisson-Boltzmann equation for biomolecular electrostatics: a tool for structural biology. *J. Mol. Recogn.* Vol. 15, No. 6, pp. 377-392, ISSN 0952-3499.

Frank-Kamenetskii, M. D. (1971). Simplification of the empirical relationship between melting temperature of DNA, its GC content and concentration of sodium ions in solution. *Biopolymers* Vol. 10, No. 12, pp. 2623-2624, ISSN 1097-0282.

Grochowski, P. & Trylska, J. (2008). Continuum molecular electrostatics, salt effects, and counterion binding – a review of the Poisson–Boltzmann theory and its modifications. *Biopolymers* Vol. 89, No. 2, pp. 93-113, ISSN 1097-0282.

Grossman, P. D. & Soane, D. S. (1991). Experimental and theoretical studies of DNA separations by capillary electrophoresis in entangled polymer solutions. *Biopolymers* Vol. 31, No. 10, pp. 1221-1228, ISSN 1097-0282.

Gruziel, M.; Grochowski, P. & Trylska, J. (2008). The Poisson-Boltzmann model for tRNA: Assessment of the calculation set-up and ionic concentration cutoff. *J. Comput. Chem.* Vol. 29, No. 12, pp. 1970-1981, ISSN 1096-987X.

Hashem, Y. & Auffinger, P. (2009). A short guide for molecular dynamics simulations of RNA systems. *Methods* Vol. 47, No. 3, pp. 187-197, ISSN 1046-2023.

Hoagland, D. A.; Arvanitidou, E. & Welch, C. (1999). Capillary electrophoresis measurements of the free solution mobility for several model polyelectrolyte systems. *Macromolecules* Vol. 32, No. 19, pp. 6180-6190, ISSN 0024-9297.

Jayaram, B. & Beveridge, D. L. (1991). Grand canonical Monte Carlo simulations on aqueous solutions of sodium chloride and sodium DNA: excess chemical potentials and sources of nonideality in electrolyte and polyelectrolyte solutions. *J. Phys. Chem.* Vol. 95, No. 6, pp. 2506-2516, ISSN 0022-3654.

Jayaram, B. & Beveridge, D. L. (1996). Modeling DNA in aqueous solutions: theoretical and computer simulation studies on the ion atmosphere of DNA. *Annu. Rev. Biophys. Biomol. Struct.* Vol. 25, No. 1, pp. 367-394, ISSN 1056-8700.

Klein, B. K.; Anderson, C. F. & Record, M. T., Jr. (1981). Comparison of Poisson-Boltzmann and condensation model expression for the colligative properties of cylindrical polyions. *Biopolymers* Vol. 20, No. 10, pp. 2263-2280, ISSN 1097-0282.

Koehl, P. (2006). Electrostatics calculations: latest methodological advances. *Curr. Opin. Struct. Biol.* Vol. 16, No. 2, pp. 142-151, ISSN 0959-440X.

Korolev, N.; Lyubartsev, A. P. & Nordenskiold, L. (2002). Application of the Poisson Boltzmann polyelectrolyte model for analysis of equilibria between single-, double-, and triple-stranded polynucleotides in the presence of K^+, Na^+, and Mg^{2+} ions. *J. Biomol. Struct. Dyn.* Vol. 20, No. 2, pp. 275-290, ISSN 0739-1102.

Korolev, N.; Lyubartsev, A. P. & Nordenskiöld, L. (1998). Application of polyelectrolyte theories for analysis of DNA melting in the presence of Na^+ and Mg^{2+} ions. *Biophys. J.* Vol. 75, No. 6, pp. 3041-3056, ISSN 0006-3495.

Krasovska, M. V.; Sefcikova, J.; Réblová, K.; Schneider, B.; Walter, N. G. & Šponer, J. (2006). Cations and hydration in catalytic RNA: molecular dynamics of the hepatitis delta virus ribozyme. *Biophys. J.* Vol. 91, No. 2, pp. 626-638, ISSN 0006-3495.

Le Bret, M. & Zimm, B. H. (1984). Distribution of counterions around a cylindrical polyelectrolyte and Manning's condensation theory. *Biopolymers* Vol. 23, No. 2, pp. 287-312, ISSN 1097-0282.

Leipply, D.; Lambert, D. & Draper, D. E. (2009). Ion-RNA interactions: thermodynamic analysis of the effects of mono- and divalent ions on RNA conformational equilibria. *Methods Enzymol.* Vol. 469, pp. 433-463, ISSN 0076-6879.

Lohman, T. M.; deHaseth, P. L. & Record, M. T., Jr. (1980). Pentalysine-deoxyribonucleic acid interactions: a model for the general effects of ion concentrations on the interactions of proteins with nucleic acids. *Biochemistry* Vol. 19, No. 15, pp. 3522-3530, ISSN 0006-2960.

Lohman, T. M. & Mascotti, D. P. (1992). Thermodynamics of ligand-nucleic acid interactions. *Methods Enzymol.* Vol. 212, pp. 400-424, ISSN 0076-6879.

MacKerell, A. D., Jr. & Nilsson, L. (2008). Molecular dynamics simulations of nucleic acid-protein complexes. *Curr. Opin. Struct. Biol.* Vol. 18, No. 2, pp. 194-199, ISSN 0959-440X.

Manning, G. S. (1969). Limiting laws and counterion condensation in polyelectrolyte solutions. I. Colligative properties. *J. Chem. Phys.* Vol. 51, No. 3, pp. 924-933, ISSN 0021-9606.

Manning, G. S. (1977). Limiting laws and counterion condensation in polyelectrolyte solutions: IV. The approach to the limit and the extraordinary stability of the charge fraction. *Biophys. Chem.* Vol. 7, No. 2, pp. 95-102, ISSN 0301-4622.

Manning, G. S. (1978). The molecular theory of polyelectrolyte solutions with applications to the electrostatic properties of polynucleotides. *Q. Rev. Biophys.* Vol. 11, No. 02, pp. 179-246, ISSN 0033-5835.

Manning, G. S. (2003). Comments on selected aspects of nucleic acid electrostatics. *Biopolymers* Vol. 69, No. 1, pp. 137-143, ISSN 1097-0282.

Manning, G. S. & Mohanty, U. (1997). Counterion condensation on ionic oligomers. *Physica A* Vol. 247, No. 1-4, pp. 196-204, ISSN 0378-4371.

Mascotti, D. P. & Lohman, T. M. (1990). Thermodynamic extent of counterion release upon binding oligolysines to single-stranded nucleic acids. *Proc. Natl. Acad. Sci. USA* Vol. 87, No. 3142, pg. 3146, ISSN 0027-8424.

Mascotti, D. P. & Lohman, T. M. (1993). Thermodynamics of single-stranded RNA and DNA interactions with oligolysines containing tryptophan. Effects of base composition. *Biochemistry* Vol. 32, No. 40, pp. 10568-10579, ISSN 0006-2960.

Mascotti, D. P. & Lohman, T. M. (1995). Thermodynamics of charged oligopeptide-heparin interactions. *Biochemistry* Vol. 34, No. 9, pp. 2908-2915, ISSN 0006-2960.

Materese, C. K.; Savelyev, A. & Papoian, G. A. (2009). Counterion atmosphere and hydration patterns near a nucleosome core particle. *J. Am. Chem. Soc.* Vol. 131, No. 41, pp. 15005-15013, ISSN 0002-7863.

Mills, P.; Anderson, C. F. & Record, M. T., Jr. (1986). Grand canonical Monte Carlo calculations of thermodynamic coefficients for a primitive model of DNA-salt solutions. *J. Phys. Chem.* Vol. 90, No. 24, pp. 6541-6548, ISSN 0022-3654.

Misra, V. K. & Draper, D. E. (1999). The interpretation of Mg^{2+} binding isotherms for nucleic acids using Poisson-Boltzmann theory. *J. Mol. Biol.* Vol. 294, No. 5, pp. 1135-1147, ISSN 0022-2836.

Misra, V. K.; Sharp, K. A.; Friedman, R. A. & Honig, B. (1994). Salt effects on ligand-DNA binding - minor-groove binding antibiotics. *J. Mol. Biol.* Vol. 238, No. 2, pp. 245-263, ISSN 0022-2836.

Mohanty, U. & Stellwagen, N. C. (1999). Free solution mobility of oligomeric DNA. *Biopolymers* Vol. 49, No. 3, pp. 209-214, ISSN 1097-0282.

Montoro, J. C. G. & Abascal, J. L. F. (1998). Ionic distribution around simple B-DNA models II. Deviations from cylindrical symmetry. *J. Chem. Phys.* Vol. 109, No. 14, pp. 6200-6210, ISSN 0021-9606.

Murthy, C. S.; Bacquet, R. J. & Rossky, P. J. (1985). Ionic distributions near polyelectrolytes. A comparison of theoretical approaches. *J. Phys. Chem.* Vol. 89, No. 4, pp. 701-710, ISSN 0022-3654.

Ni, H. H.; Anderson, C. F. & Record, M. T., Jr. (1999). Quantifying the thermodynamic consequences of cation (M^{2+}, M^{+}) accumulation and anion (X^{-}) exclusion in mixed salt solutions of polyanionic DNA using Monte Carlo and Poisson-Boltzmann calculations of ion-polyion preferential interaction coefficients. *J. Phys. Chem. B* Vol. 103, No. 17, pp. 3489-3504, ISSN 1089-5647.

Olivera, B. M.; Baine, P. & Davidson, N. (1964). Electrophoresis of the nucleic acids. *Biopolymers* Vol. 2, No. 3, pp. 245-257, ISSN 1097-0282.

Olmsted, M. C.; Anderson, C. F. & Record, M. T., Jr. (1989). Monte Carlo description of oligoelectrolyte properties of DNA oligomers: range of the end effect and the approach of molecular and thermodynamic properties to the polyelectrolyte limits. *Proc. Natl. Acad. Sci. USA* Vol. 86, No. 20, pp. 7766-7770, ISSN 0027-8424.

Olmsted, M. C.; Anderson, C. F. & Record, M. T., Jr. (1991). Importance of oligoelectrolyte end effects for the thermodynamics of conformational transitions of nucleic acid oligomers: A grand canonical Monte Carlo analysis. *Biopolymers* Vol. 31, No. 13, pp. 1593-1604, ISSN 1097-0282.

Olmsted, M. C.; Bond, J. P.; Anderson, C. F. & Record, M. T., Jr. (1995). Grand canonical Monte Carlo molecular and thermodynamic predictions of ion effects on binding of an oligocation (L^{8+}) to the center of DNA oligomers. *Biophys. J.* Vol. 68, No. 2, pp. 634-647, ISSN 0006-3495.

Owczarzy, R.; Moreira, B. G.; You, Y.; Behlke, M. A. & Walder, J. A. (2008). Predicting stability of DNA duplexes in solutions containing magnesium and monovalent cations. *Biochemistry* Vol. 47, No. 19, pp. 5336-5353, ISSN 0006-2960.

Pack, G. R.; Wong, L. & Lamm, G. (1999). Divalent cations and the electrostatic potential around DNA: Monte Carlo and Poisson–Boltzmann calculations. *Biopolymers* Vol. 49, No. 7, pp. 575-590, ISSN 1097-0282.

Paulsen, M. D.; Richey, B.; Anderson, C. F. & Record, M. T., Jr. (1987). The salt dependence of the preferential interaction coefficient in DNA solutions as determined by grand

canonical Monte Carlo simulations. *Chem. Phys. Lett.* Vol. 139, No. 5, pp. 448-452, ISSN 0009-2614.

Pérez, A.; Luque, F. J. & Orozco, M. (2007). Dynamics of B-DNA on the microsecond time scale. *J. Am. Chem. Soc.* Vol. 129, No. 47, pp. 14739-14745, ISSN 0002-7863.

Plum, G. E. & Bloomfield, V. A. (1988). Equilibrium dialysis study of binding of hexammine cobalt(III) to DNA. *Biopolymers* Vol. 27, No. 6, pp. 1045-1051, ISSN 0006-3525.

Ponomarev, S. Y.; Thayer, K. M. & Beveridge, D. L. (2004). Ion motions in molecular dynamics simulations on DNA. *Proc. Natl. Acad. Sci. USA* Vol. 101, No. 41, pp. 14771-14775.

Prabhu, V. M. (2005). Counterion structure and dynamics in polyelectrolyte solutions. *Curr. Opin. Colloid Interface Sci.* Vol. 10, No. 1-2, pp. 2-8, ISSN 1359-0294.

Putnam, C. D.; Hammel, M.; Hura, G. L. & Tainer, J. A. (2007). X-ray solution scattering (SAXS) combined with crystallography and computation: defining accurate macromolecular structures, conformations and assemblies in solution. *Q. Rev. Biophys.* Vol. 40, No. 03, pp. 191-285, ISSN 0033-5835.

Ramanathan, G. V. & Woodbury, J. (1982). Statistical mechanics of electrolytes and polyelectrolytes. II. Counterion condensation on a line charge. *J. Chem. Phys.* Vol. 77, No. 8, pp. 4133-4140, ISSN 0021-9606.

Rambo, R. P. & Tainer, J. A. (2010). Bridging the solution divide: comprehensive structural analyses of dynamic RNA, DNA, and protein assemblies by small-angle x-ray scattering. *Curr. Opin. Struct. Biol.* Vol. 20, No. 1, pp. 128-137, ISSN 0959-440X.

Record, M. T., Jr.; Anderson, C. F. & Lohman, T. M. (1978). Thermodynamic analysis of ion effects on the binding and conformational equilibria of proteins and nucleic acids: the roles of ion association or release, screening, and ion effects on water activity. *Q. Rev. Biophys.* Vol. 11, No. 02, pp. 103-178, ISSN 0033-5835.

Record, M. T., Jr.; Lohman, T. M. & Haseth, P. d. (1976). Ion effects on ligand-nucleic acid interactions. *J. Mol. Biol.* Vol. 107, No. 2, pp. 145-158, ISSN 0022-2836.

Record, M. T., Jr.; Zhang, W. & Anderson, C. F. (1998). Analysis of effects of salts and uncharged solutes on protein and nucleic acid equilibria and processes: a practical guide to recognizing and interpreting polyelectrolyte effects, Hofmeister effects, and osmotic effects of salts. *Adv. Protein Chem.* Vol. 51, pp. 281-353, ISSN 0065-3233.

Rouzina, I. & Bloomfield, V. A. (1997). Competitive electrostatic binding of charged ligands to polyelectrolytes: practical approach using the non-linear Poisson-Boltzmann equation. *Biophys. Chem.* Vol. 64, No. 1-3, pp. 139-155, ISSN 0301-4622.

Sanbonmatsu, K. Y.; Joseph, S. & Tung, C. S. (2005). Simulating movement of tRNA into the ribosome during decoding. *Proc. Natl. Acad. Sci. USA* Vol. 102, No. 44, pp. 15854-15859, ISSN 0027-8424.

SantaLucia, J. J. (1998). A unified view of polymer, dumbbell, and oligonucleotide DNA nearest-neighbor thermodynamics. *Proc. Natl. Acad. Sci. USA* Vol. 95, No. 4, pp. 1460-1465, ISSN 0027-8424.

SantaLucia, J. J.; llawi, H. T. & Seneviratne, P. A. (1996). Improved nearest-neighbor parameters for predicting DNA duplex stability. *Biochemistry* Vol. 35, No. 11, pp. 3555-3562, ISSN 0006-2960.

Sen, A.; Ray, A. & Maiti, M. (1996). Thermodynamics of the interactions of sanguinarine with DNA: influence of ionic strength and base composition. *Biophys. Chem.* Vol. 59, No. 1-2, pp. 155-170, ISSN 0301-4622.

Sharp, K. A. (1995). Polyelectrolyte electrostatics: salt dependence, entropic, and enthalpic contributions to free energy in the nonlinear Poisson–Boltzmann model. *Biopolymers* Vol. 36, No. 2, pp. 227-243, ISSN 1097-0282.

Sharp, K. A.; Friedman, R. A.; Misra, V.; Hecht, J. & Honig, B. (1995). Salt effects on polyelectrolyte–ligand binding: comparison of Poisson–Boltzmann, and limiting law/counterion binding models. *Biopolymers* Vol. 36, No. 2, pp. 245-262, ISSN 1097-0282.

Shkel, I. A. (2010). Coulombic free energy of polymeric nucleic acid: low- and high-salt analytical approximations for the cylindrical Poisson–Boltzmann model. *J. Phys. Chem. B* Vol. 114, No. 33, pp. 10793-10803, ISSN 1520-6106.

Shkel, I. A.; Ballin, J. D. & Record, M. T., Jr. (2006). Interactions of cationic ligands and proteins with small nucleic acids: analytic treatment of the large coulombic end effect on binding free energy as a function of salt concentration. *Biochemistry* Vol. 45, No. 27, pp. 8411-8426, ISSN 0006-2960.

Shkel, I. A. & Record, M. T., Jr. (2004). Effect of the number of nucleic acid oligomer charges on the salt dependence of stability (ΔG^{o}_{37}) and melting temperature (T_m): NLPB analysis of experimental data. *Biochemistry* Vol. 43, No. 22, pp. 7090-7101, ISSN 0006-2960.

Shkel, I. A.; Tsodikov, O. V. & Record, M. T., Jr. (2000). Complete asymptotic solution of cylindrical and spherical Poisson-Boltzmann equations at experimental salt concentrations. *J. Phys. Chem. B* Vol. 104, No. 21, pp. 5161-5170, ISSN 1089-5647.

Shkel, I. A.; Tsodikov, O. V. & Record, M. T., Jr. (2002). Asymptotic solution of the cylindrical nonlinear Poisson-Boltzmann equation at low salt concentration: analytic expressions for surface potential and preferential interaction coefficient. *Proc. Natl. Acad. Sci. USA* Vol. 99, No. 5, pp. 2597-2602, ISSN 0027-8424.

Slater, G. W.; Holm, C.; Chubynsky, M. V.; de Haan, H. W.; Dubé, A.; Grass, K.; Hickey, O. A.; Kingsburry, C.; Sean, D.; Shendruk, T. N. & Zhan, L. (2009). Modeling the separation of macromolecules: A review of current computer simulation methods. *Electrophoresis* Vol. 30, No. 5, pp. 792-818, ISSN 1522-2683.

Slater, G. W.; Guillouzic, S.; Gauthier, M. G.; Mercier, J.-F.; Kenward, M.; McCormick, L. C. & Tessier, F. (2002). Theory of DNA electrophoresis (~1999 - 2002 1/2). *Electrophoresis* Vol. 23, No. 22-23, pp. 3791-3816, ISSN 1522-2683.

Spasic, A. & Mohanty, U. (2008).*Counterion condensation in nucleic acid*. S. A. Rice, (Ed.), pp. 139-176, John Wiley & Sons, Inc., ISBN 9780470259498, Ithaca NY.

Stein, V. M.; Bond, J. P.; Capp, M. W.; Anderson, C. F. & Record, M. T., Jr. (1995). Importance of coulombic end effects on cation accumulation near oligoelectrolyte B-DNA: a demonstration using ^{23}Na NMR. *Biophys. J.* Vol. 68, No. 3, pp. 1063-1072, ISSN 0006-3495.

Stellwagen, N. C.; Gelfi, C. & Righetti, P. G. (1997). The free solution mobility of DNA. *Biopolymers* Vol. 42, No. 6, pp. 687-703, ISSN 1097-0282.

Stigter, D. (1995). Evaluation of the counterion condensation theory of polyelectrolytes. *Biophys. J.* Vol. 69, No. 2, pp. 380-388, ISSN 0006-3495.

Stigter, D. & Dill, K. A. (1996). Binding of ionic ligands to polyelectrolytes. *Biophys. J.* Vol. 71, No. 4, pp. 2064-2074, ISSN 0006-3495.

Strauss, U. P.; Helfgott, C. & Pink, H. (1967). Interactions of polyelectrolytes with simple electrolytes. II. Donnan equilibria obtained with DNA in solutions of 1-1 electrolytes. *J. Phys. Chem.* Vol. 71, No. 8, pp. 2550-2556, ISSN 0022-3654.

Tan, Z. J. & Chen, S. J. (2009). Predicting electrostatic forces in RNA folding. Vol. 469, pp. 465-487, ISSN 0076-6879.

Trizac, E. & Téllez, G. (2007). Preferential interaction coefficient for nucleic acids and other cylindrical polyions. *Macromolecules* Vol. 40, No. 4, pp. 1305-1310, ISSN 0024-9297.

Viovy, J. L. (2000). Electrophoresis of DNA and other polyelectrolytes: physical mechanisms. *Rev. Mod. Phys.* Vol. 72, No. 3, pg. 813, ISSN 0034-6861.

Wang, K.; Yu, Y. X.; Gao, G. H. & Luo, G. S. (2007). Preferential interaction between DNA and small ions in mixed-size counterion systems: Monte Carlo simulation and density functional study. *J. Chem. Phys.* Vol. 126, No. 13, pp. 135102-135108, ISSN 0021-9606.

Wilcoxon, J. P. & Schurr, J. M. (1983). Electrophoretic light scattering studies of poly(L-lysine) in the ordinary and extraordinary phase. Effects of salt, molecular weight, and polyion concentration. *J. Chem. Phys.* Vol. 78, No. 6, pp. 3354-3364, ISSN 0021-9606.

Williams, A. P.; Longfellow, C. E.; Freier, S. M.; Kierzek, R. & Turner, D. H. (1989). Laser temperature-jump, spectroscopic, and thermodynamic study of salt effects on duplex formation by dGCATGC. *Biochemistry* Vol. 28, No. 10, pp. 4283-4291, ISSN 0006-2960.

Wilson, W. D.; Tanious, F. A.; Barton, H. J.; Jones, R. L.; Fox, K.; Wydra, R. L. & Strekowski, L. (1990). DNA sequence dependent binding modes of 4',6-diamidino-2-phenylindole (DAPI). *Biochemistry* Vol. 29, No. 36, pp. 8452-8461, ISSN 0006-2960.

Wong, G. C. L. & Pollack, L. (2010). Electrostatics of strongly charged biological polymers: ion-mediated interactions and self-organization in nucleic acids and proteins. *Annu. Rev. Phys. Chem.* Vol. 61, No. 1, pp. 171-189.

Wu, J. & Morikis, D. (2006). Molecular thermodynamics for charged biomacromolecules. *Fluid Phase Equilib.* Vol. 241, No. 1-2, pp. 317-333, ISSN 0378-3812.

Young, M. A.; Jayaram, B. & Beveridge, D. L. (1997). Intrusion of counterions into the spine of hydration in the minor groove of B-DNA: fractional occupancy of electronegative pockets. *J. Am. Chem. Soc.* Vol. 119, No. 1, pp. 59-69, ISSN 0002-7863.

Zhang, W.; Bond, J. P.; Anderson, C. F.; Lohman, T. M. & Record, M. T., Jr. (1996). Large electrostatic differences in the binding thermodynamics of a cationic peptide to oligomeric and polymeric DNA. *Proc. Natl. Acad. Sci. USA* Vol. 93, No. 6, pp. 2511-2516, ISSN 0027-8424.

Zhang, W. T.; Ni, H. H.; Capp, M. W.; Anderson, C. F.; Lohman, T. M. & Record, M. T., Jr. (1999). The importance of coulombic end effects: experimental characterization of the effects of oligonucleotide flanking charges on the strength and salt dependence of oligocation (L^{8+}) binding to single-stranded DNA oligomers. *Biophys. J.* Vol. 76, No. 2, pp. 1008-1017, ISSN 0006-3495.

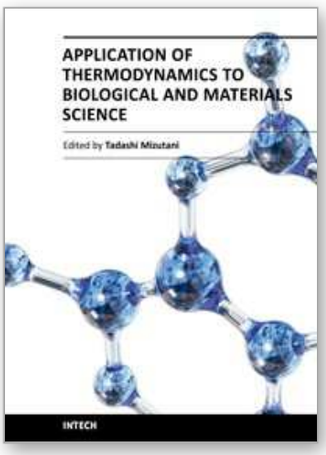

Application of Thermodynamics to Biological and Materials Science

Edited by Prof. Mizutani Tadashi

ISBN 978-953-307-980-6
Hard cover, 628 pages
Publisher InTech
Published online 14, January, 2011
Published in print edition January, 2011

Progress of thermodynamics has been stimulated by the findings of a variety of fields of science and technology. The principles of thermodynamics are so general that the application is widespread to such fields as solid state physics, chemistry, biology, astronomical science, materials science, and chemical engineering. The contents of this book should be of help to many scientists and engineers.

How to reference

In order to correctly reference this scholarly work, feel free to copy and paste the following:

Jeff D. Ballin and Gerald M. Wilson (2011). Role and Applications of Electrostatic Effects on Nucleic Acid Conformational Transitions and Binding Processes, Application of Thermodynamics to Biological and Materials Science, Prof. Mizutani Tadashi (Ed.), ISBN: 978-953-307-980-6, InTech, Available from: http://www.intechopen.com/books/application-of-thermodynamics-to-biological-and-materials-science/role-and-applications-of-electrostatic-effects-on-nucleic-acid-conformational-transitions-and-bindin

INTECH
open science | open minds

InTech Europe
University Campus STeP Ri
Slavka Krautzeka 83/A
51000 Rijeka, Croatia
Phone: +385 (51) 770 447
Fax: +385 (51) 686 166
www.intechopen.com

InTech China
Unit 405, Office Block, Hotel Equatorial Shanghai
No.65, Yan An Road (West), Shanghai, 200040, China
中国上海市延安西路65号上海国际贵都大饭店办公楼405单元
Phone: +86-21-62489820
Fax: +86-21-62489821

IntechOpen